Nivolumab reaches brain lesions in patients with recurrent glioblastoma and induces T-cell activity and upregulation of checkpoint pathways

Signe Koggersbøl Skadborg[1,10], Simone Maarup[2,3,10], Arianna Draghi[3], Annie Borch[1], Sille Hendriksen[1], Filip Mundt[4], Vilde Pedersen[2,7,8], Matthias Mann[4,9], Ib Jarle Christensen[2], Jane Skjøth-Ramussen[2,5], Christina Westmose Yde[6], Bjarne Winther Kristensen[2,7,8], Hans Skovgaard Poulsen[2], Benedikte Hasselbalch[2], Inge Marie Svane[3], Ulrik Lassen[2,10], Sine Reker Hadrup[1,10]

[1] Experimental and Translational Immunology, Department of Health Technology, Technical University of Denmark, Kgs. Lyngby, Denmark

[2] DCCC Brain Tumor Center, Department of Oncology, Copenhagen University Hospital, Rigshospitalet, Copenhagen, Denmark

[3] National Center for Cancer Immune Therapy, CCIT-DK, Copenhagen University Hospital, Herlev and Gentofte, Herlev, Denmark

[4] Novo Nordisk Foundation Center for Protein Research, CPR, University of Copenhagen, Copenhagen, Denmark

[5] Department of Neurosurgery, Copenhagen University Hospital, Rigshospitalet, Copenhagen, Denmark

[6] Center for Genomic Medicine, Copenhagen University Hospital, Rigshospitalet, Copenhagen, Denmark

[7] Department of Pathology, The Bartholin Institute, Copenhagen University Hospital, Rigshospitalet, Copenhagen, Denmark

[8] Department of Clinical Medicine and Biotech Research & Innovation Centre (BRIC), University of Copenhagen, Copenhagen, Denmark

[9]Research Department Proteomics and Signal Transduction, Max Planck Institute of Biochemistry, Martinsried, Germany

[10] These authors contributed equally: Signe Koggersbøl Skadborg, Simone Maarup, Ulrik Lassen, Sine Reker Hadrup

Corresponding Author

Sine Reker Hadrup; Henrik Dams Allé, 204, 154, 2800 Kgs. Lyngby, Denmark; E-mail: sirha@dtu.dk

Conflicts of interest

Nivolumab was provided by Bristol-Meyer Squibb. Bristol-Meyer Squibb did not exert any influence on the study and did not provide financial support for the study. SRH is the coinventor of patents WO2015185067 (Determining antigen recognition through barcoding of MHC multimers) and WO2015188839 (General detection and isolation of specific cells by binding of labeled molecules) for the barcoded MHC technology that is licensed to Immudex. IMS has received grants from or signed contracts with Bristol-Myers Squibb, Adaptimmune, IO Biotech, Lytix biopharma, TILT Biotherapeutics, and Enara Bio; has received consulting fees from MSD, IO Biotech, Novartis, Pierre Fabre, Novo Nordisk, and TILT Biotherapeutics; has received honoraria for lectures, presentations, or educational events from MSD, Novartis, Sanofi Aventis, Pierre Fabre, Bristol-Myers Squibb, IO Biotech, TILT Biotherapeutics, Novo Nordisk, and Takeda; has received support for attending meetings and/or travel from MSD; owns IO Biotech stocks.

Funding information

The work was funded by the Danish Cancer Society (R204-A12416), Læge Sofus Carl Emil Friis og Hustru Olga Doris Friis' Legat, and The Novo Nordisk Research Foundation (Challenge Grant NNF21OC0066562, Center for Nano Immune Cell Engineering (NICE)).

Running title

Nivolumab can reach GBM lesions and alter T-cell profile

Keywords

Cancer immunotherapy, Glioblastoma Multiforme, T cells, Immune Checkpoint Blockade, Neoantigens

Abstract

Glioblastoma (GBM) is an aggressive brain tumor with poor prognosis. Although immunotherapy is being explored as a potential treatment option for patients with GBM, it is unclear whether systemic immunotherapy can reach and modify the tumor microenvironment in the brain. We evaluated immune characteristics in patients receiving the anti-PD1 immune checkpoint inhibitor Nivolumab one week prior to surgery, compared to control patients receiving salvage resection without prior Nivolumab treatment. We observed saturating levels of Nivolumab bound to intratumorally- and tissue-resident T cells in the brain, implicating saturating levels of Nivolumab reaching brain tumors. Following Nivolumab treatment, significant changes in T-cell activation and proliferation were observed in the tumor resident T-cell population, and peripheral T cells upregulated chemokine receptors related to brain homing. A strong Nivolumab-driven upregulation in compensatory checkpoint inhibition molecules, TIGIT, LAG-3, TIM-3 and CTLA-4 was observed, potentially counteracting the treatment effect. Finally, tumor-reactive tumor-infiltrating lymphocytes (TILs) were found in a subset of Nivolumab-treated patients with prolonged survival, and neoantigen-reactive T cells were identified in both TILs and blood. This indicates a systemic response towards GBM in a subset of patients, which was further boosted by Nivolumab, with T-cell responses towards tumor-derived neoantigens. Our study demonstrates that Nivolumab does reach the GBM tumor lesion and enhances antitumor T-cell responses both intratumorally and systemically. However, various anti-inflammatory mechanisms mitigate the clinical efficacy of the anti-PD1 treatment.

Synopsis

The authors demonstrate that the anti-PD-1 Nivolumab can reach and modify the GBM tumor microenvironment within seven days of administration. Upregulation of compensatory immune checkpoint inhibition molecules may counter the benefits of Nivolumab-induced intratumoral immune activation.

Introduction

At primary diagnosis, patients with glioblastoma (GBM) are treated with maximal surgery, radiation and concomitant Temozolomide, also known as Stupp's regimen(1). However, when relapse occurs no standard treatment is available(2). Even though numerous treatment strategies have been explored, overall survival (OS) remains short at 14.6 months(1). Therefore, new treatment options are urgently needed, and immunotherapy is one strategy being explored that may show promise in selected patients(3,4).

The brain is typically considered an immune-privileged organ, which has been equated with the notion that there is no passage of peripheral immune cells to the parenchyma of the brain(5). However, it has been shown that communication with the peripheral immune system does occur, including cellular exchange. It is known that T cells can be primed in the meningeal area of the brain(6). However, knowledge of the route of entry and presence of effector T cells in the parenchyma or tumor tissue localized in the brain, is minimal. It has been shown in mice that cerebral spinal fluid (CSF) and interstitial fluid are drained via the central nervous system (CNS)-draining lymphatic vessels to the deep cervical lymph node, which suggests an alternative route for immune surveillance of the brain(7–9).

Immunotherapy has revolutionized cancer treatment, yet many cancer types are still unresponsive to current immunotherapeutic strategies(10–12). The effect of immune-checkpoint inhibition has been sparse in GBM, and it has been questioned if the checkpoint inhibitors pass the blood-brain barrier (BBB) sufficiently to enter the tumor microenvironment(13). The anti-PD1 immune checkpoint inhibitor Nivolumab is a molecule of 146 kDa, while only molecules of 0.4-0.5 kDa are believed to pass the BBB freely(13). It has earlier been shown that the BBB is compromised in some areas of primary brain tumors while other areas remain intact(14,15). Additionally, some GBM tumors have high collagen levels, which can challenge the penetration capacity(16). Together these characteristics may limit the penetrance of Nivolumab and effector immune cells and hence compromise the effect of immunotherapy in GBM.

Checkpoint inhibitors have shown promising results in brain cancer in mouse models(17,18), but such positive indications have not translated into treatment improvements in humans(19). Therefore, it is critical to determine if Nivolumab sufficiently enters the brain and saturates PD1 binding on T cells within GBM tumors. Here we determined the effect of Nivolumab treatment in a unique 7-day window of Nivolumab treatment prior to surgical resection. We demonstrated the presence of Nivolumab at saturated levels on tumor resident T cells, even in this short treatment window. Furthermore, treatment

mediated substantial changes in T-cell activation, proliferation, and checkpoint inhibition signatures, providing important clues to the minimal treatment effect and how to resolve this. Also, we found that T cells, both in blood and tumor, can recognize tumor-derived neoantigens, and these can be boosted by immunotherapy.

Methods and Materials

Trial design

CA209-9UP is an open label phase 2 clinical trial, designed as a trial in a real-life setting to evaluate treatment of recurrent GBM with Nivolumab and Bevacizumab under conditions close to routine practice (NCT03890952). In this study Bristol-Meyer Squibb sponsored Nivolumab. At primary diagnosis, patients received Stupp's regimen(1). Patients were treated at Rigshospitalet, Copenhagen University Hospital but the inclusion was open nationally upon transfer. In total, 44 patients were screened, 4 were screen failures, leaving 40 patients that were included in a surgical group (N=20) and non-surgical group (N=20) depending on the possibility of salvage neurosurgical resection (Figure 1a, Supplementary Figure S1). All patients received 240mg Nivolumab and 10mg/kg Bevacizumab every two weeks. The surgical group also received 240mg Nivolumab approximately 7 days prior surgery. In total 44 patients were included by January 2021, and follow-up was ended May 2022. End points were translational research, safety, and efficacy. The trial was approved by the Danish Ethical Committee (EudraCT 2017-003925-13), written informed consents were obtained from patients with the possibility to withdraw consent at any time. The study was conducted in accordance with the Declaration of Helsinki and STROBE guidelines. Age at diagnosis, performance status and multifocal disease at inclusion were registered. Extent of surgical resection was extracted from the operation note. Corticosteroid use was found in the record, medicine registry or operation note. IDH1/IDH2 mutations were investigated by immunohistochemistry and next-generation sequencing. Cut-off value for O-6-methylguanine-DNA methyltransferase (MGMT status); methylated/un-methylated was 10%. Additional inclusion and exclusion criteria are listed in Supplementary Table S1. Additionally, control patients (N=10) with recurrent GBM undergoing neurosurgical resection were included and donated fresh tumor tissue. The controls did not receive Nivolumab or Bevacizumab in the recurrent setting. Control patients provided written consent and followed our ethical guidelines according to Danish law. We used real world data as controls from our GBM database on patients from Rigshospitalet Copenhagen, we found 156 patients treated with Irinotecan and Bevacizumab at recurrent setting from 2006-2014. Gender was equally distributed, ages ranged from 23 to 79 years and median age was 58 years. Of the 156 patients, 81 patients had salvage resection while 75 patients had none. Clinical data from these patients were used as historical controls.

Statistical analyses and considerations of clinical results

The Kaplan-Meier method was used to estimate survival probabilities for overall survival (OS) as well as progression-free survival (PFS) for patients stratified by group with log rank statistics. Comparison of the

patients in the trial to the historical controls was weighted using propensity scores based on age, gender, corticosteroid use, multifocal disease, MGMT status and extent of resection. Separate analyses were done for those undergoing reoperation or not. Results were presented with 95% confidence limits and the significance level was 5%. Calculations were done using SAS (v9.4, Cary, N.C., USA). Multivariate analysis was performed using the Cox proportional hazards model with covariates; treatment group, gender, age per 10 years, MGMT status, corticosteroid use.

Patient material

RNA/DNA extraction from tumor tissue or blood

Samples from tumors were available from the surgical group; recurrent tumor samples were collected and stored in RNAlater (Thermo Fischer Scientific) immediately after resection. Archival tissue from autologous primary tumor was available as fresh frozen tissue or formalin fixed paraffin embedded (FFPE) tissue. Blood samples for germline DNA were collected in Streck- and EDTA vials. DNA and RNA were extracted from fresh frozen tissue using the AllPrep RNA/DNA/Protein Mini Kit (Qiagen). RNA was further DNase treated with RNeasy mini kit (Qiagen). DNA and RNA were extracted from FFPE slides by GeneRead DNA FFPE kit (Qiagen) and Agencourt FormaPure Reagent Kit (Beckman Coulter), respectively. DNA from blood for germline whole exome sequencing (WES) was extracted by ReliaPrep Large Volume HT gDNA isolation system (Promega). Manufacturers' instructions were followed for all kits. Bioanalyzer 2100 with the 6000 RNA Nano and Pico Assay was used to evaluate the RNA quality. RNA was quantified using DeNovix Spectrophotometer. DNA was quantified using Qubit Fluorometric Quantification (Thermo Fisher Scientific). Library preparation for WES was done by SureSelect Clinical Research Exome (Agilent). Library preparation for bulk RNAseq was performed using TruSeq Stranded total RNA kit (Illumina) with unique dual indexes (UDIs). Each sample was sequenced once and QC controlled to ensure >50x coverage for WES samples, and >50 mill reads and >50% mRNA content for RNAseq, respectively. All sequencing was performed on Illumina NovaSeq 6000 (Illumina) using 2 x 150 bp paired-end sequencing.

Peripheral blood mononuclear cells (PBMCs)

Peripheral blood samples were collected from patients at several time points (Figure 1a): baseline (day 0, prior to treatment), after 8 weeks and after 16 weeks. One additional blood sample was collected 3 weeks after Nivolumab administration in the surgical group – two weeks after surgery. PBMCs were

isolated using Lymphoprep density gradient (Takeda) and cryopreserved in 10% DSMO (Herlev Hospital Pharmacy) and 90% human serum (Sigma-Aldrich/Merck KGaA) using controlled-rate freezing (Cool-Cells, Biocision) in -80 °C, and later stored in -140 °C (Figure 1a).

In vitro expansion of tumor-infiltrating lymphocytes

Minimally expanded young tumor-infiltrating lymphocytes (YTILs) were obtained from resected tumor tissue. In brief, tumor tissue was cut into 1-3 mm^3 fragments and plated in wells of a 24 well-plate with 2 mL complete medium consisting of 90% RPMI-1640 plus GlutaMAX and 25 mM HEPES (Gibco, Thermo Fisher Scientific), 10% heat-inactivated human AB serum (Sigma-Aldrich/Merck KGaA, Darmstadt, Germany), 100 U/mL penicillin, 100 µg/mL streptomycin (Pen/Strep, Gibco, Thermo Fisher Scientific, Waltham, MA), 1.25 µg/mL Amphotericin B (Fungizone®, Bristol-Myers-Squibb), and 6,000 IU/mL of rhIL-2 (Proleukin®, Novartis). Plates were incubated at 37 °C with 5% CO_2 and were inspected every other day from day five to investigate extrusion and proliferation of lymphocytes. Half of the medium was replaced with fresh complete medium every other day after day 5. Cells were split when needed, harvested after 3-6 weeks, and cryopreserved as described above(20,21).

Rapid expansion protocol (REP) TILs were expanded from YTILs (just harvested or thawed). When biopsies were sparse, REP TILs were prioritized over young TILs due to a higher success rate in production of REP TILs than YTILs. Frozen YTILs were thawed and cultured in complete media for 48 hours prior rapid expansion. During rapid expansion, 100,000 YTILs were co-cultured with feeder cells and 30ng/mL anti-CD3 (clone OKT-3, Miltenyi Biotec) in 10mL complete medium and 10mL rapid expansion medium, which consisted of AIM-V (Thermo Fisher Scientific) and Fungizone® 1.25 µg/ml supplemented with 6,000 IU rhIL-2/ml in T25 flasks (Thermo Fischer Scientific). Feeder cells (PBMCs) from minimum six donors were thawed and irradiated by 40 Gy (Gammacell 3000 Elan, MDS Nordion). REP cultures were incubated at 37 °C with 5% CO_2 for 5 days. On day 5 of the rapid expansion, half of the medium was replaced with 10mL of mixed medium (consisting of 1:1; complete medium:rapid expansion medium). According to growth, the cultures were moved to larger flasks and rapid expansion medium was added over the next 9 days. On day 14+1, REP TILs were harvested and cryopreserved as mentioned above(20,21).

Tumor digest (single-cell suspension)

Fresh tumor samples from the operating theater were transported in medium (RPMI-1640 plus GlutaMAX and 25mM HEPES) (Gibco, Thermo Fisher Scientific) supplemented with Pen/Strep (Gibco,

Thermo Fisher Scientific) on ice. The fresh tumor tissue was dissected under sterile conditions into fragments after the macroscopical vessels were removed. Tumor fragments were then placed in a T80 flask with 25 mL of digesting medium consisting of 100 mL RPMI-1640 plus GlutaMAX and 25mM HEPES supplemented with 1% Pen/Strep, 1 mg/mL Collagenase (Cat No C5138-100MG, Sigma-Aldrich), 0.025 mg/mL Dornase alfa (Pulmozyme®, Genentech), and placed overnight on a magnetic stirrer at room temperature. After minimum of 18 hours the digested tumor fragments were filtered through a 70 µM filter to obtain a single-cell suspension. The single cells were cryopreserved as aforementioned.

An overview of the cell and tumor digest samples used in the study is shown in Supplementary Table S2.

Immunohistochemistry

FFPE GBM tissue from patients and controls were cut on a microtome (2 µm). The 10 controls had pathologically verified GBM and used a maximum of 20 mg prednisolone, comparable to the inclusion criteria in the trial. Tissue sections were deparaffinized and subject to heat-induced epitope retrieval with either Cell Conditioner 1 for 84 minutes at 100°C (CD3, PD-1 and IgG4) or EnVision TRS low pH, 40 minutes at 97°C (PD-L1). Endogenous peroxidase activity was blocked with EnVision FLEX Peroxidase-Blocking Reagent (Agilent Technologies). Incubation with CD3 Ready-To-Use (RTU) antibody (clone: 2GV6, Roche), PD-1 antibody (clone: MRQ22, Roche) diluted in EnVision FLEX Antibody Diluent K8006 and IgG4 antibody (clone: MRQ44, Cell Marque) diluted in the same diluent was done using the BenchMark ULTRA Platform (Ventana Medical Systems) with the OptiView DAB IHC Detection system (Roche Diagnostics). Incubation with PD-L1 RTU antibody (clone: 22C3, Dako) was done using the Dako Omnis Platform (Agilent Technologies) using the EnVision FLEX DAB+ Chromogen (Dako Omnis) detection system. Nuclei were counterstained with hematoxylin. Unregistered fully anonymized human tonsil samples were used as controls and stained as above. Slides were evaluated using a BX51 microscope (Olympus Danmark A/S, Ballerup, Denmark), and reviewed by neuropathologist co-author BWK. Slides were digitalized using the NanoZoomer XR digital image scanner (Hamamatsu, Japan).

Phenotyping by flow cytometry

Cryopreserved PBMCs, YTILs, REP TILs and tumor digest were thawed and washed once in RPMI 1640 Medium with 10% fetal bovine serum (FBS, Gibco, Thermo Fisher Scientific) for cellular staining. Tumor digest was thawed and rested overnight in X-vivo 15 (Lonza) with 5% heat-inactivated sterile filtered human serum (HS, Sigma-Aldrich) to regain surface-marker expression after enzymatic digestion. PBMCs, YTILs and REP TILs were thawed immediately before staining. PBMC and tumor digest were

washed twice in PBS with 2% FBS (FACS buffer), stained with a panel of fluorochrome conjugated antibodies for surface markers (Supplementary Table S3 indicates the different panels of antibodies used for flow cytometry analysis) for 30 minutes (dark, 4 °C), and cells were washed twice in FACS buffer. For staining of intracellular (ICS) markers in antibody panels B, C and D, we used the eBioscience™ Foxp3/Transcription Factor Staining Buffer Set (Invitrogen) following the manufacturer's protocol. Fixation/permeabilization working solution was added to surface stained PBMCs and tumor digest and incubated overnight (dark, 4 °C). Cells were washed twice in 1X Permeabilization Buffer and antibodies for intracellular markers were added and cells were stained for 30 minutes and hereafter washed twice with 1X Permeabilization Buffer. PBMCs and digest stained with panel A (surface markers only) were fixed in 1% PFA. Samples were resuspended in FACS buffer and acquired on an LSRFortessa (BD bioscience). Phenotype analysis was performed once for each patient sample.

Analysis of flow cytometry data

Tumor digest contained much debris and lymphocyte counts varied between patients. Samples with less than 30 events in the parent populations ($CD4^+$ T cells or $CD8^+$ T cells) were not included in the analysis. Number of events in parent population per patient samples are shown in Supplementary Figure S2a. Flow cytometry data was analyzed in FlowJo v10.8.1. Manual gating was performed as depicted in Supplementary Figure S2b.

TIL Reactivity Assay

YTILs and REP TILs were tested for reactivity against autologous tumor digest with cytokine intracellular staining. TILs were thawed in pulmozyme buffer (RPMI-1640 plus GlutaMAX and 25mM HEPES) (Gibco, Thermo Fisher Scientific) supplemented with Pen/Strep (Gibco, Thermo Fisher Scientific), 0.5mL of Magnesium chloride (Herlev Hospital Pharmacy and 0.025 mg/mL dornase alfa (Pulmozyme®, Genentech)) washed and cultured in RPMI+ Pen/Strep+ 10% HS with a concentration of 2-4x10^6 cells/mL. TILs were rested overnight at 37 °C, 5% CO_2. Tumor digests were thawed in transport medium and washed. Cells from tumor digests were counted and resuspended in RPMI-1640+ Pen/Strep+ 10% HS at a concentration of 2x10^6 cells/mL. TILs were washed and resuspended in RPMI-1640+ Pen/Strep+ 10% HS at a concentration of 3x10^6 cells/mL. TILs and digest T cells were co-cultured in a ratio of 3:1 by adding 100µL TILs suspension and 50µL autologous tumor digest suspension per well in a sterile 96 well plate (Thermo Scientific). GolgiPlug (BD Biosciences), GolgiStop (BD Biosciences) and anti-CD107a (BD Biosciences) were added according to manufacturer's recommendations and RPMI-1640+ Pen/Strep+

10% HS was added up to a total volume of 200µL per well. TILs stimulated with PMA/ionomycin (25ng/0.5uM) (Sigma Aldrich/Sigma Aldrich) or 0.4uL Leukocyte Activating Cocktail (BD Biosciences) were used as positive controls. TILs alone were used as negative controls. Melanoma or colorectal carcinoma tumor cell lines without MHC-I and II expressions due to *B2M* or *CIITA* knockout by CRISPR-associated protein 9 (CAS9) were additionally used as negative controls, both previously described(20,22)(See *Control tumor cell lines*). The co-cultures were incubated for 8 hours in a humidified incubator 37°C with 5% CO_2 and then stained as described above (see *Phenotyping by flow cytometry*) using antibody panels C or D (Supplementary Table S3). Stained cells were acquired on an LSRFortessa or NovoCyte Quanteon Flow Cytometer (Agilent, Sata Clara, CA) and analyzed with FlowJo 10.6.1 or 10.8.1. Reactivity assays were repeated for verification of results.

Control tumor cell lines

Short-term (<10 passages) *in vitro* cultured tumor cell lines were established via serial passage of adherent cells from tumor fragments in RPMI-1640 plus GlutaMAX and 25mM HEPES (Cat. No 72400-021, Gibco, Thermo Fisher Scientific) supplemented with Pen Strep, 10% FBS (Cat. No 10270106, Gibco, Thermo Fisher Scientific) and 500 ng/ml of Hydrocortison (Solu-Cortef®, Pfizer). All tumor cell lines were generated internally and authenticated via *in vitro* patterns of growth, morphology (light microscopy), and when in doubt, expression of lineage antigens by PCR. Mycoplasma testing (Cat. No A3744.0020, VWR International) was routinely performed according to manufacturer's instructions. No Mycoplasma infection was detected in the past six years. Established tumor cells were cultured in RPMI-1640 plus GlutaMAX and 25mM HEPES supplemented with Pen Strep and 10% of FBS. To abrogate the expression of MHC molecules, the tumor cell lines were subjected to CRISPR-Cas9-mediated knockout of *B2M* or *CIITA,* as previously described in detail(22). crRNAs targeting the *B2M* (5´- CAGTAAGTCAACTTCAATGT-3') and *CIITA* (5´-GATATTGGCATAAGCCTCCC-3`) genes were selected from the literature(23) or designed using the Custom Alt-R® CRISPRCas9 guide RNA design tool (Integrated DNA Technologies). sgRNAs and S.p. HiFi Cas9 Nuclease V3 were purchased from Integrated DNA Technologies' Alt-R catalog, and ribonucleoprotein (RNP) complexes were formed as per the manufacturer instructions. 40,000 tumor cells were then seeded in a well of a 96-well plate with flat bottom and transfected with RNP complexes at a concentration of 10 nmol/L using Lipofectamine CRISPRMAX Cas9 Transfection Reagent (Cat No CMAX00008, Thermo Fisher Scientific) following the manufacturer's instructions. After at least 72hrs, the cells were treated for additional 72 hrs with 100 IU/mL IFNg (Cat No 300–02, Peprotech) to induce MHC molecules upregulation. The loss of MHC molecules expression was verified by flow cytometry.

Purified *B2M* KO and *CIITA* KO populations were generated by electronic sorting on a BD FACS Melody Cell Sorter (BD Biosciences) and further expanded. In the experiments performed in this study, the purified populations were further cultured before testing for less than two months, or maximum 10 additional passages.

Transcriptomics

Preprocessing of the RNA sequencing FASTQ files was done using trimming with TrimGalore 0.6.4 (24) which was combined with Cutadapt(25) and FastQC version 0.11.9(26). Kallisto Quant version 0.46.0(27) was used to align the trimmed reads to GRCh38(28). The Kallisto output was used as input to estimate the cell population with the Microenvironment cell population counter (MCP-counter) version 1.2.0 (https://genomebiology.biomedcentral.com/articles/10.1186/s13059-016-1070-5).

Proteomic analyses

Sample preparation for mass spectrometry-based

Frozen tumor tissue were processed by Qiagen© AllPrep DNA/RNA/Protein Mini Kit for protein purification. The final flow-through containing the proteins was processed through acetone precipitation as previously described(29). The resulting protein pellet was re-suspended in 200 µl, 8 M urea, in Tris-HCl (pH 8.0), supplemented with PhosSTOP (Roche) and Complete Protease Inhibitor (Sigma Aldrich), following the manufacturers' instructions. The pellet was completely dissolved by pipetting and sonication (Bioruptor®, Diagenode; 5 times 30 seconds on and 30 seconds off cycles). Protein concentrations were determined, and protein solutions were reduced and alkylated as described, followed by tryptic digest and peptide clean up on two 14-gauge styrene divinylbenzene reverse phase sulfonate StageTip plugs using a previously described protocol(29,30). Clean peptides were resuspended in 10 µL 0.1 % formic acid and analyzed on a NanoDrop™ for their concentrations as before.

Mass spectrometry analyses

A total of 200 ng clean peptides were loaded on C18 Evotips (EvoSep) following manufacturer's protocol. Briefly, tips were wetted in isopropanol for 10 seconds, and then activated with 20 µL 100 % acetonitrile with 1 % formic acid. Evotips were cleared by one minute centrifugation at 800 round centrifugal force (rcf) and again wetted in isopropanol for 10 seconds. Then the Evotips were conditioned with 20 µL of 0.1 % formic acid and cleared for one minute at 800 rcf before 200 ng of samples were loaded and spun down (800 rcf for one minute). We loaded a total of 300 ng of de-salted peptides per sample on each

tip. Tips were then washed once with 20 µL of 0.1 % formic acid and centrifuged at 800 rcf for one minute, before being stored with 100 µL of 0.1% formic acid on the tips and plenty of 0.1 % formic acid in the Evotip box to prevent drying. The charged tips were loaded on an EvoSep One liquid chromatographer (EvoSep) and injected at a rate of 30 samples per day, i.e., with a 44-minute gradient. Samples were analyzed on a TimsTOF Pro (Bruker) using diaPASEF acquisition mode. The column used was commercially pre-packed with 1.5 µm C18-beads (PepSep) with the following dimensions: 15 cm × 150 µm inner diameter. Column was heated to 40°C during the runs. For reference of the original diaPASEF method, please see Meier et al.(31). Mass spectrometry diaPASEF raw files were searched with DIA-NN software (version 1.8). Samples were searched against the human FAST files (9606), which were in silico digested for library free searches and library generation. Missed cleavages were set to 1, and number of allowed variable modifications to 2. N-terminal methionine excision, carbamidomethylation of cysteines, oxidation of methionine and N-terminal acetylation were selected as modifications. Peptide lengths were allowed within, and including, 7 to 30 amino acid residues. Precursor charge range was set to 2 to 4, precursor m/z range from 100 to 1700, and fragment ion m/z range from 200 to 1800. Mass accuracy and MS1 accuracy were both set to 15.0, matches between runs were enabled and likely interferences were removed. Data was re-searched in a second pass using the on-the-fly generated spectral library. For more details see DOI: https://doi.org/10.1101/2023.05.12.540582 (29). Data was log2-transformed and median-MAD (median absolute deviation) normalized (robust z-scores) before bioinformatical analyses.

Differential expression analysis

Differential expression analysis (DEA) for proteomics and transcriptomics was performed with DeSeq2 version 1.30.1(32). The results with genes and log-fold change were used as input to a Gene Set Enrichment Analysis (GSEA) with clusterprofiler packages from R version 4.2.2(33) and both the Gene Ontology database (GO) and Kyoto encyclopedia of genes and genomes (KEGG) database was applied. Complexity heatmap version 2.10(34) was used for the heatmap and enrich figures were made with geasqplot2 from enrichplot(35).

Detection of Neoantigen-reactive T-cells in PBMCs and TILs

Neoantigens were predicted from the WES data. The mutations were detected by the GATK4 best practice(36). Firstly, the WES reads were trimmed using TrimGalore 0.6.4(24) combined with Cutadapt (25) and FastQC 0.11.9(26) with a minimum length of 50 bp, and other default settings. The trimmed

reads were aligned to the human reference genome, GRCh38(28) using BWA-MEM 0.7.16a(37) followed by the pre-processing steps including MarkDuplicate and base re-calibrator(36). Somatic variant calling was performed using MuTect2(38), with filtering of panel of normal (PON) and contamination filter from GTAK best practice. MuPexi(39) were used to predict neoepitope candidates, which were filtered by the expression of the corresponding gene obtained from kaillisto version 0.46.0(27) and the binding to the corresponding HLA-allele predicted with NetMHCPan 4.1(40). The patient specific HLA-alleles were typed used Razers3 (version 3.4)(41) followed by OptiType version 1.2(42). The criteria for selecting neoepitope candidates were expression level >= 0.1 TPM and then top 100 of the best EL%Rank to the HLA allele but only including HLA binders. Neoantigens were predicted for both primary and recurrent tumors.

PBMCs, YTILs and REP TILs were screened once for neoantigen-reactive $CD8^+$ T cells (NARTs) and virus antigen–reactive T cells (VARTs) using in-house assembled DNA barcode-labelled peptide-MHC-I (pMHC) multimers(43). In short DNA barcode-labelled peptide-MHC-I multimers were assembled so each DNA barcode was specific for each pMHC in the neoantigen panel (Supplementary Table S4). The multimers were built on a streptavidin-conjugated dextran backbone labelled with a fluorochrome (NARTs: PE, VARTs: APC)(FINA biosolutions LCC). Predicted neoantigen peptides (Pepscan) were loaded in their respective biotinylated MHC monomers (produced in-house). Biotinylated DNA barcodes (produced in-house) and biotinylated pMHC were bound to the flourochrome-conjugated dextran-backbone via the streptavidin binding sites. Patient samples were stained with a patient specific pool of pMHC multimers, together with CD8 and CD3 antibodies (Supplementary Table S3). PE and APC labelled $CD8^+$ T cells were then sorted by fluorescence activating cell sorting (FACS) on a FACSAria (BD). DNA barcodes in the sorted cells were then amplified by PCR. A baseline sample from the multimer pool was also amplified as a reference. PCR products were sequenced by Primbio and sequencing results were analysed in Barracoda. Production and downstream application of DNA barcoded-labelled pMHC multimers is thoroughly described by Bentzen et al.(43). Output files from Barracoda included information on the fold change of enriched DNA barcodes in the sorted samples compared to the baseline and whether the enrichment was significant. A fold change (log2) over 2 and $p < 0.001$ was set as threshold for a significantly enriched DNA barcode, at which point, the T-cell recognition of the pMHC was annotated.

Verification peptide reactivity

Peptides detected by NARTs were verified by peptide-specific expansion of patient PBMCs. PBMCs were co-cultured with a pool of reactive peptides for 14 days. PBMCs were cultured in X-vivo (Lonza) with 5%

human serum. Peptides were added at day 0 with a concentration of 10 ug/ml per peptide. PBMCs were additionally stimulated with 40 IU/ml IL-2, and 0.5ug/ml purified anti-CD28 (BD, clone: CD28.2). Medium with IL-2 was changed twice per week. To validate the pMHC specificity of the given T-cell cultures PBMCs expanded with peptides were stained with single tetramers produced in-house. 400 uM DMSO dissolved peptides (Pepscan) were mixed with in their respective biotinylated MHC monomers (produced in-house (43)) with a concentration of 200 ug/mL in a volume 1:1 resulting in final concentrations of 200uM peptides and 100 ug/mL MHC monomers. Peptide exchange is performed via UV radiation (366 nm) for 1 hour. The pMHCs are hereafter mixed with fluorochrome-conjugated streptavidin (final concentration 0.018 ug/uL, PE and APC, Biolegend), and hereafter incubated for 30 min on ice in the dark. 0.056 uL 500uM D-biotin (Avidity) pr 1 uL pMHC-streptavidin product and 10X freezing buffer (PBS with 5% BSA, Sigma Aldrich and 50% glycerol, Sigma Aldrich) is added, and tetramers were hereafter stored at -20 degrees. For staining of PBMCs. Each tetramer was fluorochrome labelled with both PE and APC. Expanded PBMCs were washed twice in FACS buffer, and hereafter stained with 2 uL tetramer (1 uL APC conjugated and 1 uL PE conjugates) and PBS was added up to a total staining volume of 80 uL. PBMCs were incubated for 15 min at 37°C in the dark. 20ul Ab mix containing CD3-FITC, CD8-BV480, CD4-BUV394 and NiR (See Supplementary Table S3 for information) were added and incubated on ice for 30 min in the dark. The samples were washed twice in FACS buffer and were analyzed using an LSRFortessa (BD) and FlowJo v10.

Statistical analysis

For bar plots, unpaired t-test was used to compare means of two groups and performed with a 95% confidence interval. * = $p<0.05$, ** = $p<0.01$, *** = $p<0.001$, **** = $p<0.0001$. Other statistical analyses are described in detail in the given method section.

Data availability statement

The data generated in this study are available within the article and its supplementary data files, or can be obtained from the corresponding author upon reasonable request. Raw patient data cannot be shared freely due to the constraints of the informed consent and regulations stipulated by Danish and EU law. Each request for data use must undergo assessment and validation to ensure compliance with the consent and legal provisions. Raw sequencing data is stored at the Danish National Genome Center and can be shared upon appropriate data access agreement. The Danish National Genome Center has provided an online guide for applying for data access, available at: https://www.eng.ngc.dk/research-

and-international-collaboration/dngc-research-services/how-to-apply-for-access. Patient IDs used in the study can be obtained from the authors, following the data access application.

Results

Tumor and peripheral blood were collected to analyze Nivolumab's immune effects in GBM patients

CA209-9UP is an open-label phase 2 clinical study in which 44 patients with recurrent GBM following Stupp's regimen(1) were included from November 2018 to January 2022. 4 patients became screen failures, while 40 patients were treated with Nivolumab (PD-1 inhibitor) and Bevacizumab (anti-VEGF-A) every 14 days. The patients were divided in two groups; 20 patients received a first dose of 240 mg Nivolumab 7 days before salvage resection as a window of opportunity to study treatment effects in tumor tissue (surgical group), while 20 patients were considered non-operable (non-surgical group) (Figure 1a, Supplementary Figure S1). Additionally, we included 10 control patients with recurrent GBM, not treated with Nivolumab or Bevacizumab, to investigate if Nivolumab could influence the immune-cellular signatures at the tumor site in recurrent GBM patients (Figure 1a). Tumor and blood samples were collected as illustrated in Figure 1a.

Nivolumab and Bevacizumab treatment provide no apparent survival benefit for patients with GBM

The 40 patients included in the CA209-9UP clinical trial for evaluation of Nivolumab and Bevacizumab treatment had a median age at diagnosis of 57.5 years (surgical group) and 50.5 years (non-surgical group). For both patient groups, 77% (31 out of 40 patients) did not receive corticosteroids at inclusion (Supplementary Table S5). The 10 control patients had a median age of 57 years and 90% of the control patients did not receive corticosteroids at inclusion (1 out of 10 patients) (Supplementary Table S5). Tumor samples were historically verified as GBM, however today, 8 CA209-9UP patients (3 surgical and 5 non-surgical group) and 2 controls would classify as astrocytoma, IDH-mutant, WHO grade IV according to WHO's recent classification of brain tumors(2,44). The tumor classification changed in 2021 after the onset of this clinical trial. The patient groups had equal distributions of gender, performance status and corticosteroid usage, while 45% of patients in the surgical group harbored un-methylated MGMT compared to 55% in the non-surgical group. Fewer of the control patients were MGMT unmethylated (20%), and more had a total resection (90%), while the extent of disease was similar to the CA209-9UP patients (Supplementary Table S5). Overall, the treatment was well tolerated. One suspected unexpected serious adverse reaction (SUSAR) of posterior reversible encephalopathy syndrome (PRES) was reported and the patient was excluded from further treatment. Serious adverse events of grade 3 and 4 (CTCAE version 4.03) are listed in Supplementary Table S6.

For all patients in CA209-9UP, we observed a median overall survival (mOS) of 10.9 months (7.0-14.1) and median progression free survival (mPFS) of 4.1 months (3.8-5.9). When stratified, the surgical and non-surgical group had a mPFS of 6.0 and 3.8 months, respectively, while the mOS was 14.0 months and 6.4 months, respectively. mOS follow-up was 30.0 months (15.2–40.1) and 27.2 months (16.0–41.0) in the surgical and non-surgical group, respectively. Multivariate analysis was performed by the following variables: corticosteroid use, MGMT status, gender, age at diagnosis, and treatment group (Supplementary Table S7). Corticosteroid use at inclusion was a significant negative predictor of outcome (p=0.04). In a follow-up survival analysis, we removed these patients, but no difference was observed, compared to the results from the whole group. We then stratified on differences in corticosteroid use at baseline (N=40) and saw that corticosteroid-using patients had mOS of 7.3 months compared to non-corticosteroid-using patients with mOS of 12.2 months.

To evaluate the potential effect of Nivolumab and Bevacizumab treatment, real-world data on the historical patient group was extracted from our one-site GBM database, from which we have reported before(45). Using real-world data as controls is an established method that has previously been used(46). The historical patient group comprised patients treated with Bevacizumab and Irinotecan and possibly neurosurgical resection (N=156; 81 patients had a neurosurgical resection, 75 patients did not). The historical surgical group (N=81) had a mOS of 9.8 months, compared to the mOS of 14.0 months in our Nivolumab/Bevacizumab-treated surgical patient group. While a marginal difference was initially observed between the two groups (log-rank of p=0.08) (Figure 1b), no difference was observed (log-rank p-value=0.46) (Figure 1c) when the patient cohorts were matched based on propensity scores, including relevant clinical and performance characteristic. In the non-surgical group, matched historical patients (N=75) had a mOS of 7.0 months, while mOS was 6.4 months in the Nivolumab/Bevacizumab-treated patient group. Hence no difference was observed, neither without, nor with, matching based on propensity score (log-rank of p= 0.77 and p=0.11, respectively) (Figure 1d and e).

When comparing survival (PFS and OS from recurrence) of the surgical group (NIVO) to control patients used for immunological analyses, no difference in survival was observed (Supplementary Figure S3). In conclusion, we found no survival benefit among patients treated with Nivolumab and Bevacizumab compared to matched historical patients. However, we did observe five long-term survival patients (>20 months after tumor recurrence) in the Nivolumab/Bevacizumab-treated group. The length of survival was unexpected based on clinical parameters, such as time from primary diagnosis to progression (4.8 months, 6.7 months, 4.9 months, 14.8 months, and 8.7 months) and MGMT- or IDH-status (two MGMT

unmethylated, one IDH mutated), and hence may indicate clinical effect of Nivolumab treatment in selected cases.

Nivolumab can be found in GMB brain lesions and saturates PD-1 expressed on intratumoral T cells

Tumor samples were analyzed to evaluate if Nivolumab can penetrate to the brain and reach the tumor site in sufficient amount to saturate PD-1 binding on T cells. To detect Nivolumab binding to PD-1 on T-cell surfaces, we applied a fluorochrome-conjugated anti-IgG4, the isotype of Nivolumab, while free PD-1 molecules were determined by a regular fluorochrome-conjugated anti-PD-1 (Figure 2a). Tumor digests were rested overnight to re-express certain T-cell surface markers lost during tissue digestion. Before rest, T cells were only binding anti-IgG4, indicating all PD-1 molecules were bound to Nivolumab. After rest, T cells bound both anti-PD-1 and anti-IgG4, indicating surface presence of new PD-1 molecules during the resting period, or loss of Nivolumab binding. Intratumoral T cells from control patients only bound anti-PD-1, confirming that IgG4 binding is specific to Nivolumab and the PD-1 molecules on unrested T cells were intact after the enzymatic digestion (Figure 2b and 2c). Together, this demonstrates that surface expressed PD1 on intratumoral T cells are fully saturated with Nivolumab after only 7 days of treatment, and that Nivolumab must be present in an unbound form in the tumor microenvironment to capture recent surface mobilized PD-1.

Tumor digests were stained for CD69 and CD103, markers that when co-expressed identify tissue residency, to determine whether T cells in the tumor digest included tissue-resident T cells. Both markers were expressed on both $CD4^+$ and $CD8^+$ T cells in the tumor digest, with no difference in frequencies between NIVO and control patients (Figure 2d). A large fraction of the tissue-resident CD103 and CD69 co-expressing T cells were also saturated for Nivolumab-binding, exclusively in the treated patients (Figure 2e-f). This further supports the notion that Nivolumab enters the GBM lesion primarily as free molecules, and any contribution from peripheral T cells binding to Nivolumab and migrating to the tumor is minimal.

We also performed single staining for CD3, PD-1 and IgG4 of consecutive paired FFPE slides from primary and recurrent NIVO tumors. In this analysis, three patients were identified with distinct $PD\text{-}1^+$ and $IgG4^+$ cells in the recurrent tumors after Nivolumab treatment, while FFPE sections from the corresponding untreated primary tumors were $IgG4^-$ (Supplementary Figure S4). Despite not being able to perform multicolor staining of the FFPE slides, these data support our results obtained in the flow cytometry–based analysis of tumor digest.

Altogether, this suggests that Nivolumab entered the brain lesions and penetrated the tumor tissue as free immunoglobulins, in sufficient levels to saturate PD1 expression on intratumoral T cells, only 7 days after administration.

Nivolumab mediates CNS homing and profound T-cell activation in GBM

After establishing that Nivolumab penetrated the GBM tissue, we evaluated the influence on T-cell composition and signatures in NIVO patients compared to the control patients. No overall differences in the frequencies of $CD4^+$ and $CD8^+$ T cells within the T-cell compartment was observed between the two groups (Figure 3a). Additionally, when looking into the overall immune cell representation (including T cells, B cells, fibroblasts, monocyte lineage cells, myeloid dendritic cells (mDCs) etc) using the MCP-counter tool to analyze transcriptomic data, no difference was found between NIVO and control patients (Supplementary Figure S5a)

We further examined T-cell expression of markers related to migration, activation and late differentiation using multi-color flow cytometry. The chemokine receptors CD183 (CXCR3) and CD195 (CCR5) have previously been correlated with CNS homing in neurological inflammation(47,48). With inflammation considered a hallmark of cancer(49), we investigated the expression of these two chemokine receptors. The frequency of $CD4^+$ T cells co-expressing CD183 and CD195 was higher in Nivolumab-treated tumors compared to controls, while stable for $CD8^+$ T cells (Figure 3b). Furthermore, a significant increase in frequency of T cells expressing high levels of CD183 and CD195, respectively, was found on $CD4^+$ and the same tendency was observed among $CD8^+$ T cells in tumors of NIVO patients compared to the control patients. Increased expression of these chemokine receptors suggests a treatment-related effect (Figure 3c-d). An example of gating for T cells expressing higher levels of chemokine receptors are shown in figure 3e. This coincided with a trend toward lower frequencies of both $CD4^+$ and $CD8^+$ T cells co-expressing these chemokine receptors in peripheral blood (Supplementary Figure S6). Together, this suggests that Nivolumab can reinforce CNS T-cell recruitment. When looking into peripheral T cells in the entire Nivolumab/Bevacizumab-treated patient cohort, we found that PBMCs from the non-surgical group had significantly higher frequencies of $CD183^+CD195^+$ T cells within the $CD8^+$ T-cell population at baseline (day 0) and week 16 compared to the surgical group (Figure 3f). The larger fraction of cells with this migratory phenotype suggests a more pronounced neurological inflammation in patients where the tumor is maintained, and hence directly affected by the tumor milieu. Finally, a high frequency of T-cell co-expression of CD183 and CD195 also positively

correlated with the MCP-counter score for mDCs, which could be responsible for the recruitment of T cells (Supplementary Figure S5b).

As we found a CNS homing signature among T cells in both blood and tumor, we further evaluated the activation status of intratumoral T cells after Nivolumab treatment. A significantly enhanced proliferation was observed among both intratumoral $CD8^+$ and $CD4^+$ T cells following Nivolumab treatment, based on the detection of Ki67 expression (Figure 3g). Furthermore, the frequency of T cells expressing the co-stimulatory molecule CD28, did not change significantly following treatment (Figure 3h), but patients with a higher frequency of $CD8^+$ T cells expressing CD28 tended to have longer PFS and OS after recurrence, but only among NIVO patients (Supplementary Figure S7) suggesting co-stimulation might influence T-cell behavior in Nivolumab-treated patients.

Among the tissue-resident T cells expressing CD103 and CD69, the co-expression of CD39, a marker of recent T-cell activation, was only observed among NIVO patients (Figure 3i, Supplementary Figure S6). A similar tendency was found within $CD4^+$ T cells but at a much lower frequency level (Figure 3h). Furthermore, expression of the early activation marker CD137 (4-1BB) tended to increase in tissue-resident $CD8^+$ T cells after Nivolumab treatment (Figure 3j).

Signatures of immune modulation were likewise apparent from transcriptomic data obtained from resected tumor material of the NIVO and control group. From a differential expression analysis (DEA), genes related to inflammation, including *FOXA* and *CXCL17*, and *FGFBP2*, a gene related to T-cell effector function, were significantly overexpressed in the NIVO group. However, most other significantly overexpressed genes were related to cancer progression (*MT-RNR1*, *SNOR7A*, *MIR663B*, *MIR6087*, *FGG*, *FGA*, *HMGCS2*, *PIP*, *REG1A*) rather than immune response signatures (Figure 3k, Supplementary Figure S8).

Taken together, a profound signature of T-cell activation and proliferation was observed in GBM tumors 7 days after Nivolumab treatment.

Nivolumab treatment induces strong compensatory upregulation of immune-inhibitory pathways

In addition to the T-cell activation signature observed following Nivolumab treatment, upregulation of co-inhibitory molecules was identified. Significantly higher frequencies of both $CD8^+$ and $CD4^+$ T cells expressing TIGIT, LAG-3, TIM-3 (CD8+) and CTLA-4 were found in tumor tissue from NIVO patients compared to untreated control patients (Figure 4a-d). Limited differences were observed in PBMCs for these markers before and after Nivolumab administration (Supplementary Figure S6), suggesting a

tumor-specific effect. In addition, the frequencies of intratumoral $CD8^+$ and $CD4^+$ T cells expressing two or more of the inhibitory molecules, TIGIT, LAG-3, TIM-3 and CTLA-4, was significantly larger within the NIVO patients compared to the control patients (Figure 4e, Supplementary Figure S9). Specifically, the frequency of quadruple positive $CD8^+$ T cells was significantly higher in NIVO patient, along with significantly higher frequencies of intratumoral T cells that were double positive for TIGIT and LAG-3 ($CD4^+$ and $CD8^+$) and for TIGIT and TIM-3 ($CD8^+$) (Supplementary Figure S9). This suggests a major impairment of intratumoral T-cell function following Nivolumab treatment. Finally, the level of regulatory T cells (Tregs) was low in tissue from controls, but highly heterogeneous between NIVO patients (Figure 4f), suggesting that also this T-cell subset may be altered.

The frequency of peripheral $CD8^+$ T cells expressing TIGIT in the non-surgical group was found to be significantly higher at week 16 compared to the surgical group (Figure 4g). This could indicate an ongoing exhaustion of T cells in the non-surgical group, as the tumor was still present, and suggesting that chronic inflammation within the tumor tissue could be monitored by a peripheral upregulation of TIGIT.

While upregulation of compensatory co-inhibitory molecules was observed, the level of PD1 expression was decreased following Nivolumab treatment. Intratumoral $CD8^+$ T cells expressing PD-1 were found in significantly lower frequencies in NIVO patients compared to the control patients, and a similar trend was shown within intratumoral $CD4^+$ T cells (Figure 4h). Furthermore, a significant drop in frequencies of peripheral PD-1-expressing $CD8^+$ T cells was observed after Nivolumab treatment, and a similar trend was shown within peripheral $CD4^+$ T cells (Figure 4i). PD-1 expression was measured using both anti-PD-1 and anti-IgG4 staining. The kinetics of Nivolumab binding are shown in Figure 4j, where PBMC-derived $CD8^+$ T cells were stained with anti-PD-1 and anti-IgG4. At baseline, PD-1 molecules on T cells were stained only by anti-PD-1, while after Nivolumab administration, PD-1 molecules were instead stained by anti-IgG4. The sum of the T-cell populations stained by either anti-PD-1 or anti-IgG4 was therefore defined as the total $PD\text{-}1^+$ population (PD-1), to compare expression of PD-1 between time points and patient groups.

Thus, our data demonstrates that the T-cell activation signature observed following Nivolumab treatment coincided with a profound upregulation of the checkpoint-inhibition molecules TIGIT, LAG-3, TIM-3 and CTLA-4 on tumor-infiltrating T cells, while the expression of PD1 declined after treatment initiation. The overall change in T-cell phenotypes following Nivolumab treatment remained when excluding data from patients now classified as astrocytoma, IDH-mutant, WHO grade IV (Supplementary

Figure S10). Finally, no difference in these results was observed when removing patients receiving corticosteroid from analyses (Supplementary Figure S11).

Tumor reactivity is detected in TILs from a fraction of patient with a distinct inflammatory profile

To further investigate the tumor-recognition capacity of immune cells from Nivolumab-treated patients, we tested the intracellular cytokine signature of expanded TILs when co-cultured with autologous tumor digest. Reactivity of REP TILs against autologous tumor digest was demonstrated in four Nivolumab-treated patients (NVB02, NVB05, NVB08, NVB10) out of 16 tested patients. REP TILs from patients NVB02 and NVB05 showed clear tumor recognition responses among both $CD4^+$ and $CD8^+$ T cells. For patient NVB10, we detected a small response only among $CD8^+$ T cells in REP TILs (Figure 5a, Supplementary Figure S12 and S13a). Overall tumor reactivity ranged between 1.2-13.6% of $CD8^+$ TILs and between 6.3-10.9 % of $CD4^+$ TILs (Figure 5a). To assess whether T-cell reactivity could influence patient outcome, we calculated the mOS and mPFS of the patients with reactive T cells to be 17.0 months and 9.3 months, respectively. These were numerically higher compared to the NIVO patients without tumor-reactive TILs, mOS of 12.8 months and mPFS of 4.3 months (Supplementary Figure S13b). However, the difference was not significant due to the small study cohort applicable to TIL reactivity analyses, and the results warrant further studies.

Transcriptomics analyses were performed to investigate differences in the TME between patients with tumor-reactive TILs, and the rest of the surgical group within the Nivolumab-treated patients. The DEA showed 1,522 differentially expressed genes and large differences in the TME were observed, revealing a cluster-split dividing patients with tumor-reactive versus tumor non-reactive TILs (Figure 5b). The overexpressed genes observed in the patients with reactive TILs included *TGFB1*, *CXCL13* and *IL31RA*, which are all related to inflammation (Figure 5b). In addition, from a GSEA, we identified differential overexpression of the MHC class I (MHC-I) peptide presentation pathway in patients with tumor-reactive TILs (Figure 5c), which was supported by higher HLA class I expression among tumor digest–derived live cells from patients with tumor-reactive TILs (Supplementary Figure S14). The cluster-split dividing patients with tumor-reactive versus tumor non-reactive TILs was additionally confirmed in a proteomics analysis (Supplementary Figure S15). Additionally, when assessing the T-cell characteristics, we observed a tendency for higher frequencies of T cells expressing CD28 as well as T cells expressing the inhibitory receptor TIGIT in tumors from patients with reactive TILs compared to the remaining NIVO patients

(Supplementary Figure S13c). Furthermore, a significantly higher frequency of Tregs among $CD4^+$ T cells was detected in patients with tumor-reactive TILs (Supplementary Figure S13c). In summary, the TME of the patients with tumor-reactive TILS had a different gene-expression profile than the remaining NIVO patients, and an expression suggesting stronger T-cell activation and antigen presentation yet counterbalanced by inhibitory TIGIT expression and Treg presence.

Tumor-specific NARTs are present in tumor and periphery of GBM patients

There has been limited exploration of the antigen landscape of relevance for T-cell recognition of GBM. Therefore, we aimed to determine if tumor recognition could be driven by tumor mutation–derived neoepitopes. To determine if neoepitopes could be targets for tumor-cell recognition by T cells in patients with tumor-reactive TILs, we screened for the presence of NARTs in both TILs and PBMCs, during treatment. Neoepitopes were predicted from the WES and RNA sequencing from the primary and recurrent tumors. We screened PBMCs, YTILs and REP TILs for $CD8^+$ T-cell recognition of neoepitopes using this personalized library of predicted neoepitopes and a pool of virus-derived epitopes, selected based on the patients HLA profile, to determine the level of virus antigen reactive $CD8^+$ T cells as a comparator. The screening was conducted using fluorescent and DNA barcode-labelled pMHC multimers, allowing pooling of 134-183 neoepitope pMHC multimers (PE labeled) and 3-16 virus-derived pMHC multimers (APC labeled) per sample (Figure 6a). We identified NART populations against 2-6 neoepitope-MHC per patient in PBMCs and/or TILs (Figure 6b, Supplementary Figure S16). This level of recognition was comparable to other cohorts of patients, with urothelial carcinoma and melanoma, respectively, previously evaluated for NARTs(50,51), despite the overall lower tumor mutational burden in GBM tumors. The total numbers of responses across all evaluated patients are shown in Figure 6c, and the sum of estimated frequencies of NARTs and virus antigen reactive $CD8^+$ T cells is shown in Figure 6d, both for each blood sample and for the TILs. When studying the dynamics of the NARTs, there was an increased breadth of neoepitope recognition after Nivolumab treatment (week 3) in patients NVB02 and NVB05, which thereafter persisted. The same pattern was observed for the magnitude of the T-cell responses (i.e., the sum of estimated frequencies) at week 3 and week 8, especially for NVB02. NART responses were only found at baseline and at week 8 in PBMCs from NVB10. However, the breadth and magnitude appeared to increase at week 8. Neoepitope responses were only detected in TILs from NVB02 and NVB05, where both the breadth and magnitude increased in REP TILs compared to YTILs, most dominant in TILs from NVB02. The number of responses towards virus peptides in PBMCs remained consistent throughout the treatment period, as did the magnitude of these. All T-cell

responses were confirmed by a 14 day-patient-specific peptide stimulation of PBMCs (Supplementary Figure S17).

In summary, we screened for NARTs in YTILs, REP TILs and PBMCs. We found NARTs in TILs from NBV02 and NVB05. Even though the sum of estimated frequencies of detected NART was low in these patients, it coincided with NVB02 and NVB05 having the highest frequencies of reactive $CD8^+$ TILs upon tumor challenge, while NVB10 had relatively few tumor-reactive $CD8^+$ TILs, and NVB08 had no tumor-reactive $CD8^+$ TILs (Figure 5a). Thus, tumor mutation–derived neoepitopes do appear to constitute a fraction of the tumor-reactive response, and such T-cell responses were also detected in the periphery.

We further observed that the patients with tumor-reactive $CD8^+$ TILs (NVB02, NVB05, NVB10) were those with the highest proportional overlap of mutations when comparing primary and recurrent tumor (Supplementary Figure S18a), suggesting that such recognition may be dominated by clonal neoantigen recognition. In addition, we observed three neoepitopes recognized by NARTs in patient NVB05 (LLILGIYST-A0201, LARVLVTLL-B5101, RVLVTLLIL-C0102), which originated from the same frameshift mutation from the gene; *NF1* (Supplementary Figure S18b), suggesting extraordinary immunogenicity of this genetic alteration, which opens a possibility to explore this further as a potential shared neoantigen source.

Discussion

We report data from a translational phase 2 clinical study where we treated patients with recurrent GBM with Nivolumab and Bevacizumab every two weeks until progression, death, or intolerable toxicity. We showed that it was feasible and safe to use Nivolumab and Bevacizumab in this setting, but we could not demonstrate any direct benefit of Nivolumab combined with Bevacizumab on PFS or OS, when compared to historical control or when compared to control patients included in the immune analyses. The small cohort size could potentially mask survival benefits from the given treatment, as Cloughesy et al. have previously shown that neoadjuvant anti-PD-1 therapy extended survival compared adjuvant anti-PD-1 therapy(52). We did observe a few patients who unexpectedly, based on existing clinical parameters, became long-term survivors, which could indicate therapeutic benefit in a subset of patients. Moreover, this study additionally offered a unique opportunity to explore the immune infiltration to GBM tumors, and the potential impact of Nivolumab treatment on the immune landscape.

Researchers are still in the early stages of understanding the immune system of the brain, and little is known about the peripheral immune cells' role in the brain. We examined intratumoral T cells in patients with recurrent GBM, by evaluating the cellular impact of Nivolumab treatment. Moreover, we studied the effect of Nivolumab and Bevacizumab treatment on peripheral T cells in patients who did (surgical group) and did not (non-surgical group) receive resection of their recurrent tumor.

Importantly, we were able to detect Nivolumab in brain tumors only 7 days after administration to the patient, documenting the capacity for such antibodies to penetrate to this challenging location. However, it can be questioned whether Nivolumab entered as free molecules or bound to T cells. The BBB strongly regulates passage of large molecules and cells into the brain tissue through tight junction(13), but it has also been shown that the BBB in GBM can be disrupted and become more permeable in these tight junctions, which supports both scenarios(14,15). We found that PD-1 molecules on all intratumoral T cells were saturated by Nivolumab in unrested tumor digest, this also included tissue-resident T cells within tumor tissue. This implies that Nivolumab can penetrate the tumor as free immunoglobulins. Previously, *Osa et al.* showed that, when Nivolumab-pretreated T cells were cultured in Nivolumab-free medium for more than 24 hours, the Nivolumab bound to the T cells where lost. Moreover, they also showed that decreased concentrations of Nivolumab in plasma correlated with drop in level of Nivolumab-bound T cells in blood from patients with non-small cell lung cancer(53). Considering the findings of *Osa et al.*, our results indicate that Nivolumab has been in excess

in the TME as intratumoral T cells were saturated by Nivolumab, which further support the notion that Nivolumab can enter the GBM microenvironment as an immunoglobulin alone.

We found that Nivolumab treatment affected T-cell phenotypic characteristics, both in the tumor and in the periphery, and moreover we could observe an effect on the TME based on RNA sequencing of tumor tissue. Intratumoral T cells exhibited elevated CD183 and CD195 chemokine receptor expression following Nivolumab administration. Previous studies have shown CD195 and CD183 T-cell co-expression in CSF and PBMCs of patients with neurological inflammation, distinguishing them from non-inflammatory neurological diseases(47,48). Our findings suggest that Nivolumab treatment induces increased neuro-inflammation, potentially enhancing recruitment to the GBM tumor. Additionally, Nivolumab/Bevacizumab-treated patients who retained their tumor showed higher frequencies of $CD8^+$ T cells expressing CD183 and CD195 in the blood compared to the patients who underwent tumor resection. This observation supports the idea of active recruitment of peripheral T cells to the brain due to neurological inflammation, even in the context of cancer. However, further investigation is warranted to assess the presence of CNS homing T cells in both blood and CSF in the two patient groups. Furthermore, in Nivolumab-treated patients, intratumoral T cells demonstrated increased activation signatures, expression of CD39 and CD137, compared to control patients, which potentially indicates an enrichment of tumor-reactive T cells. CD39, when co-expressed with CD103, has previously been associated with extended survival in patients with head and neck cancer(54). We observed that $CD39^+$ tissue-resident $CD8^+$ T cells were more prevalent in tumor digest from Nivolumab-treated patients compared to control patients. Increased frequencies of CD39 expressing T cells can furthermore indicate an increased tumor-specific T-cell activation, as CD39 has previously been suggested as a marker to differentiate tumor-specific T calls from bystander T cells within the TME(55). While CD39 is expressed late and upon T-cell activation, CD137 expression both increases and attenuates quickly after T-cell antigen recognition and stimulation (56–60). We found a trend for increased expression of CD137 on tissue-resident $CD8^+$ T cells after Nivolumab treatment. Such cells were present at low frequencies, which could be explained by the transient expression kinetics of CD137 expression(57). Collectively, PD-1-blockade likely resulted in increased TCR activation of intratumoral T cells, also supported by overexpression of *FGFBP2*, a gene linked to T-cell cytotoxicity(61,62). Moreover, the co-stimulatory molecule CD28 was expressed on intratumoral T cells with varying frequencies among $CD8^+$ T cells within Nivolumab-exposed tumors. Previous studies have shown that $CD28^+$ T cells respond well to anti-PD-1 therapy and that loss of CD28 on $CD8^+$ T cells is a marker for unresponsive patients(63,64). We observed that a high frequency of intratumoral $CD28^+CD8^+$ T cells correlated with longer PFS and OS

after recurrence only in Nivolumab-treated patients, suggesting CD28 to be a marker of favorable T-cell response also in GBM. PD-1 acts primarily by inhibiting the co-stimulatory signal through CD28, rather than TCR signaling(65). It is possible that Nivolumab not only blocks the inhibitory signaling through PD-1, but also enables T cells to upregulate CD28 expression, and thus facilitates co-stimulation. This co-stimulation and activation may lead to expansion and proliferation of tumor-specific T-cell clones, a notion supported by the higher frequency of $Ki67^+$ intratumoral T cells we observed within Nivolumab-treated patients. Previous studies have shown that TILs in GBM exhibit a highly exhausted phenotype, primarily reflected in the high expression of PD1(66,67), but despite the enhanced intratumoral T-cell activation and proliferation following Nivolumab treatment, an anti-inflammatory TME also appeared to be augmented, perhaps as a feedback mechanism in response to an increased immune activation caused by PD-1 blockade. Upregulation of several other inhibitory molecules, LAG-3, TIM-3, CTLA-3 and TIGIT, was found to be occur on intratumoral T cells following Nivolumab and thus contribute to drug-resistance(68). In particular, TIGIT was expressed on a larger fraction of T cells and could serve as a relevant co-target as has previously been suggested(69,70). We observed that the frequency of $PD\text{-}1^+CD8^+$ T cells decreased following Nivolumab treatment both in tumor and in the periphery. This could be due to endocytosis of the receptor after Nivolumab binding, as the case is for other receptors after engagement of their target(71,72), but it needs to be evaluated further. Upregulation of additional inhibitory receptors could be a compensatory mechanism upon PD-1 downregulation. Overall, our T-cell phenotypic findings are consistent with recent research by Lee et al., who observed heightened T-cell infiltration, elevated expression of neuroinflammation-associated chemokines (XCL1, XCL2, and CCL5), and upregulation of genes related to T-cell activation and exhaustion, including TIGIT, in response to neoadjuvant anti-PD-1 treatment(73). Collectively, this indicates a positive effect of neoadjuvant therapy within this tumor type. Moreover, our study demonstrates T-cell activation and TME modulation occurring within a considerably short period of only 7 days from Nivolumab administration to tumor resection, while other neoadjuvant anti-PD1 clinical studies show the effect 14 days after administration(52,73–75). However, it becomes evident that combinatorial therapy is necessary to effectively counteract inhibitory and anti-inflammatory mechanisms induced upon anti-PD-1 treatment.

Beyond T-cell phenotyping, we were able to detect tumor reactivity in REP TILs from 25% (4 out of 16) of Nivolumab-treated patients. We found a clear difference in the TME landscape of patients with tumor-reactive TILs compared to the remaining Nivolumab-treated patients based on transcriptomic data. Specifically, we found gene set enrichment of an immune-related pathway involved in antigen processing and presentation of MHC-I. This could indicate an active immune reaction with INFγ release,

which is known to induce HLA expression(76), resulting in ongoing presentation of potential immunogenic neoepitopes to T cells within the TME of these patients, providing a potential for $CD8^+$ T cell–mediated cancer-cell killing(77,78). We therefore examined the tumor specificity of the reactive TILs further by screening PBMCs and TILs for the presence of NARTs. We were able to detect NARTs in TILs from two patients, which corresponded to the patients who showed the highest reactivity against tumor. Yhe NARTs detected in these patients (NVB02 and NVB05) were specific to neoantigens found in both the primary and recurrent tumor, potentially representing clonal mutations. In fact, we detected three immunogenic neoepitopes from patient NVB05 derived from a frameshift mutation in *NF1*. Mutations in the *NF1* gene have been reported in 13-14% of GBM, hereof 78% consisting of frameshifts(79). Additionally, *NF1* mutations have been described to be related to high T-cell infiltration in gliomas(80). Therefore, such mutations could be of interest as potential biomarkers for use in immunotherapy treatment. Consistent with this, the T-cell infiltration and quality of neoantigens, and thereby the potential to induce a potent tumor specific T-cell response has previously been correlated with longer survival for GBM patients (81). Our results support this with a higher PFS and OS after recurrence for patients with tumor-reactive TILs, compared to the remaining patients in the Nivolumab-treated group, though it was not significant in this small patient group. Personalized neoantigen vaccines have been tested to induce and boost the NART repertoire in GBM patients, but despite tumor infiltration of vaccine-induced NARTs, immune suppressive factors diminished the immune response(82,83).

Finally, an increasing number of observations suggest that the peripheral immune system plays a role in the immunosurveillance of the brain(6–9). We detected the same NART populations in both blood and tumor samples, confirming an interaction between the brain tumor and the peripheral immune system. This is consistent with a study identifying GBM-specific NARTs in blood (84), while Lee et al. showed an overlap in TCR repertoire in activated/exhausted T cells within PBMCs and TILs (73). Moreover, we found that both the number and the sum of estimated frequency of the NARTs increased after Nivolumab treatment. This aligns with previous observations from other cancer cohorts, where therapy targeting the PD-1/PD-L1 axis resulted in a boost of the number NARTs in PBMC shortly after treatment initiation(50).

In conclusion, we report that Nivolumab can penetrate GBM tumors, likely as a free molecule. Within a timeframe of only 7 days, Nivolumab induced notable changes in intratumoral T-cell phenotypes and in the gene expression profile of the TME. Additionally, we identified neoantigen-reactive $CD8^+$ T cells in

tumor-reactive TILs and in PBMC and these NARTs appeared to be boosted after Nivolumab administration. Altogether, our data, together with other neoadjuvant studies, suggest that to improve immunotherapies for GBM it is of foremost important to consider the complexity of the tumor and the resistance mechanism(s) induced after PD-1.

Acknowledgements

We thank all patients who donated material that was used in this study; the funding that supported this research; Group leader, MD, PhD M. Donia and MD and M. Presti for invaluable support and critical review of the manuscript and assistant with laboratory work; PhD T. Tamhane and A. D. E. G. Burkal for production of MHC class I monomers; B. Rotbøl and A.F. Løye for technical assistance handling the flow cytometry instruments and samples; O. S. G. Heiede for technical assistance with flow cytometry analysis. The work was funded by the Danish Cancer Society (R204-A12416), Læge Sofus Carl Emil Friis og Hustru Olga Doris Friis' Legat, The Novo Nordisk Research Foundation (Challenge Grant NNF21OC0066562, Center for Nano Immune Cell Engineering (NICE)) and Bristol-Myers Squibb generously provided Nivolumab

Author contributions

SKS study design, performing experiments, analysis and interpretation of data, generation of figures and tables, statistical analysis, writing manuscript; SM study design, collection of patient samples, performing experiments, analysis of data, generation of figures and tables, writing manuscript; AD study designed, performing experiments, data analysis; AB prediction of neoepitopes, bioinformatics analyses and generation of figures; SH bioinformatics analyses and generation figures; FM study designed and performing experiments, analysis of data; MM study designed and performing experiments, analysis of data; JSR study supervision and data discussion; CWY providing WES- and RNA-seq data; HSP conceiving study concept, patient contact, funding, study supervision and data discussion; BH conceiving study concept, patient contact, funding, study supervision, data discussion; IMS conceiving study concept, funding, study supervision, data discussion; UL conceiving study concept, patient contact, study supervision, data discussion, funding support; SRH conceiving study concept, study supervision, data discussion, funding, writing manuscript. IJC: critical review of data and managing statistical design and analyses. VP: Support, managing and evaluation of histological (FFPE) sections. BWK: Support, managing and evaluation of histological (FFPE) sections as well as funding for pathological analyses.

References

1. Stupp R, Mason WP, van den Bent MJ, Weller M, Fisher B, Taphoorn MJB, et al. Radiotherapy plus Concomitant and Adjuvant Temozolomide for Glioblastoma. N Engl J Med. 2005;352(10):987–96.

2. Wen PY, Weller M, Lee EQ, Alexander BM, Barnholtz-Sloan JS, Barthel FP, et al. Glioblastoma in adults: a Society for Neuro-Oncology (SNO) and European Society of Neuro-Oncology (EANO) consensus review on current management and future directions. Neuro Oncol. 2020;22(8):1073.

3. Schalper KA, Rodriguez-Ruiz ME, Diez-Valle R, López-Janeiro A, Porciuncula A, Idoate MA, et al. Neoadjuvant nivolumab modifies the tumor immune microenvironment in resectable glioblastoma. Nat Med. 2019;25(3):470–6.

4. Arrieta VA, Chen AX, Kane JR, Kang SJ, Kassab C, Dmello C, et al. ERK1/2 phosphorylation predicts survival following anti-PD-1 immunotherapy in recurrent glioblastoma. Nat cancer. 2021;2(12):1372.

5. Medawar PB. Immunity to Homologous Grafted Skin. III. The Fate of Skin Homographs Transplanted to the Brain, to Subcutaneous Tissue, and to the Anterior Chamber of the Eye. Br J Exp Pathol. 1948;29(1):58.

6. Bartholomäus I, Kawakami N, Odoardi F, Schläger C, Miljkovic D, Ellwart JW, et al. Effector T cell interactions with meningeal vascular structures in nascent autoimmune CNS lesions. Nature. 2009;462(7269):94–8.

7. Louveau A, Smirnov I, Keyes TJ, Eccles JD, Rouhani SJ, Peske JD, et al. Structural and functional features of central nervous system lymphatic vessels. Nature. 2015;523(7560):337–41.

8. Aspelund A, Antila S, Proulx ST, Karlsen TV, Karaman S, Detmar M, et al. A dural lymphatic vascular system that drains brain interstitial fluid and macromolecules. J Exp Med. 2015;212(7):991–9.

9. das Neves SP, Delivanoglou N, Da Mesquita S. CNS-Draining Meningeal Lymphatic Vasculature: Roles, Conundrums and Future Challenges. Front Pharmacol. 2021;12.

10. Nayak L, Molinaro AM, Peters K, Clarke JL, Jordan JT, de Groot J, et al. Randomized Phase II and Biomarker Study of Pembrolizumab plus Bevacizumab versus Pembrolizumab Alone for Patients

with Recurrent Glioblastoma. Clin Cancer Res. 2021;27(4):1048–57.

11. Reardon DA, Kim TM, Frenel JS, Simonelli M, Lopez J, Subramaniam DS, et al. Treatment with pembrolizumab in programmed death ligand 1–positive recurrent glioblastoma: Results from the multicohort phase 1 KEYNOTE-028 trial. Cancer. 2021;127(10):1620–9.

12. Larkin J, Chiarion-Sileni V, Gonzalez R, Grob J-J, Rutkowski P, Lao CD, et al. Five-Year Survival with Combined Nivolumab and Ipilimumab in Advanced Melanoma. N Engl J Med. 2019;381(16):1535–46.

13. Pluim D, Ros W, van Bussel MTJ, Brandsma D, Beijnen JH, Schellens JHM. Enzyme linked immunosorbent assay for the quantification of nivolumab and pembrolizumab in human serum and cerebrospinal fluid. J Pharm Biomed Anal. 2019 Feb 5;164:128–34.

14. Liebner S, Fischmann A, Rascher G, Duffner F, Grote EH, Kalbacher H, et al. Claudin-1 and claudin-5 expression and tight junction morphology are altered in blood vessels of human glioblastoma multiforme. Acta Neuropathol. 2000;100(3):323–31.

15. Wolburg H, Wolburg-Buchholz K, Kraus J, Rascher-Eggstein G, Liebner S, Hamm S, et al. Localization of claudin-3 in tight junctions of the blood-brain barrier is selectively lost during experimental autoimmune encephalomyelitis and human glioblastoma multiforme. Acta Neuropathol. 2003;105(6):586–92.

16. Pointer KB, Clark PA, Schroeder AB, Salamat MS, Eliceiri KW, Kuo JS. Association of collagen architecture with glioblastoma patient survival. J Neurosurg. 2017;126(6):1812.

17. Reardon DA, Gokhale PC, Klein SR, Ligon KL, Rodig SJ, Ramkissoon SH, et al. Glioblastoma eradication following immune checkpoint blockade in an orthotopic, immunocompetent model. Cancer Immunol Res. 2016;4(2):124–35.

18. Park J, Kim CG, Shim JK, Kim JH, Lee H, Lee JE, et al. Effect of combined anti-PD-1 and temozolomide therapy in glioblastoma. Oncoimmunology. 2018;8(1).

19. Reardon DA, Brandes AA, Omuro A, Mulholland P, Lim M, Wick A, et al. Effect of Nivolumab vs Bevacizumab in Patients With Recurrent Glioblastoma: The CheckMate 143 Phase 3 Randomized Clinical Trial. JAMA Oncol. 2020;6(7):1003–10.

20. Donia M, Junker N, Ellebaek E, Andersen MH, Straten PT, Svane IM. Characterization and

comparison of “standard” and “young” tumour-infiltrating lymphocytes for adoptive cell therapy at a Danish translational research institution. Scand J Immunol. 2012;75(2):157–67.

21. Andersen R, Borch TH, Draghi A, Gokuldass A, Rana AHM, Pedersen M, et al. T cells isolated from patients with checkpoint inhibitor-resistant melanoma are functional and can mediate tumor regression. Ann Oncol. 2018;29(7):1575–81.

22. Draghi A, Chamberlain CA, Khan S, Papp K, Lauss M, Soraggi S, et al. Rapid Identification of the Tumor-Specific Reactive TIL Repertoire via Combined Detection of CD137, TNF, and IFNγ, Following Recognition of Autologous Tumor-Antigens. Front Immunol. 2021 Oct 11;12:4236.

23. Abrahimi P, Chang WG, Kluger MS, Qyang Y, Tellides G, Saltzman WM, et al. Efficient gene disruption in cultured primary human endothelial cells by CRISPR/Cas9. Circ Res [Internet]. 2015 Jul 3 [cited 2022 Aug 18];117(2):121–8. Available from: https://www.ahajournals.org/doi/abs/10.1161/CIRCRESAHA.117.306290

24. Krueger F. Trim Galore [Internet]. 2019 [cited 2022 Feb 7]. Available from: https://github.com/FelixKrueger/TrimGalore

25. Martin M. Cutadapt removes adapter sequences from high-throughput sequencing reads. EMBnet.journal. 2011;17(1).

26. Andrews S. FastQC [Internet]. 2019 [cited 2022 Feb 7]. Available from: https://www.bioinformatics.babraham.ac.uk/ projects/fastqc

27. Lab P. Kallisto [Internet]. 2019 [cited 2022 Feb 9]. Available from: https://pachterlab.github.io/kallisto/

28. Consortium GR. Genome Reference Consortium Human Build 38 patch release 14 (GRCh38.p14) [Internet]. 2022 [cited 2022 Jul 4]. Available from: https://www.ncbi.nlm.nih.gov/assembly/GCF_000001405.40

29. Mundt F, Nielsen AB, Duel JK, Yde CW, Eriksen MA, Lassen U, et al. In depth profiling of the cancer proteome from the flowthrough of standard RNA-preparation kits for precision oncology. bioRxiv. 2023;2023.05.12.540582.

30. Geyer PE, Kulak NA, Pichler G, Holdt LM, Teupser D, Mann M. Plasma Proteome Profiling to Assess Human Health and Disease. Cell Syst. 2016;2(3).

31. Meier F, Brunner AD, Frank M, Ha A, Bludau I, Voytik E, et al. diaPASEF: parallel accumulation–serial fragmentation combined with data-independent acquisition. Nat Methods. 2020;17(12).

32. Love MI, Huber W, Anders S. Moderated estimation of fold change and dispersion for RNA-seq data with DESeq2. Genome Biol. 2014;15(12).

33. Wu T, Hu E, Xu S, Chen M, Guo P, Dai Z, et al. clusterProfiler 4.0: A universal enrichment tool for interpreting omics data. Innov. 2021;2(3).

34. Gu Z, Eils R, Schlesner M. Complex heatmaps reveal patterns and correlations in multidimensional genomic data. Bioinformatics. 2016;32(18).

35. Yu G. Visualization of functional enrichment result. R package version 1.10.2. Mol Ther Nucleic Acids. 2021;

36. McKenna A, Hanna M, Banks E, Sivachenko A, Cibulskis K, Kernytsky A, et al. The Genome Analysis Toolkit: a MapReduce framework for analyzing next-generation DNA sequencing data. Genome Res. 2010;20.

37. Li H. Aligning sequence reads, clone sequences and assembly contigs with BWA-MEM. arXiv Prepr arXiv. 2013;

38. Cibulskis K, Lawrence MS, Carter SL, Sivachenko A, Jaffe D, Sougnez C, et al. Sensitive detection of somatic point mutations in impure and heterogeneous cancer samples. Nat Biotechnol. 2013;31(3).

39. Bjerregaard AM, Nielsen M, Hadrup SR, Szallasi Z, Eklund AC. MuPeXI: prediction of neo-epitopes from tumor sequencing data. Cancer Immunol Immunother. 2017 Sep 1;66(9):1123–30.

40. Reynisson B, Alvarez B, Paul S, Peters B, Nielsen M. NetMHCpan-4.1 and NetMHCIIpan-4.0: Improved predictions of MHC antigen presentation by concurrent motif deconvolution and integration of MS MHC eluted ligand data. Nucleic Acids Res. 2021;48(W1).

41. Weese D, Holtgrewe M, Reinert K. RazerS 3: Faster, fully sensitive read mapping. Bioinformatics. 2012;28(20).

42. Szolek A, Schubert B, Mohr C, Sturm M, Feldhahn M, Kohlbacher O. OptiType: precision HLA typing from next-generation sequencing data. Bioinformatics. 2014;30(23):3310.

43. Bentzen AK, Marquard AM, Lyngaa R, Saini SK, Ramskov S, Donia M, et al. Large-scale detection of antigen-specific T cells using peptide-MHC-I multimers labeled with DNA barcodes. Nat Biotechnol. 2016 Oct 1;34(10):1037–45.

44. Louis DN, Perry A, Wesseling P, Brat DJ, Cree IA, Figarella-Branger D, et al. The 2021 WHO classification of tumors of the central nervous system: A summary. Neuro Oncol. 2021;23(8).

45. Basch E, Schrag D. The Evolving Uses of "Real-World" Data. Vol. 321, JAMA. 2019.

46. Urup T, Dahlrot RH, Grunnet K, Christensen IJ, Michaelsen SR, Toft A, et al. Development and validation of a prognostic model for recurrent glioblastoma patients treated with bevacizumab and irinotecan. Acta Oncol (Madr). 2016;55(4).

47. Giunti D, Borsellino G, Benelli R, Marchese M, Capello E, Valle MT, et al. Phenotypic and functional analysis of T cells homing into the CSF of subjects with inflammatory diseases of the CNS. J Leukoc Biol. 2003;73(5):584–90.

48. Teleshova N, Pashenkov M, Huang YM, Söderström M, Kivisäkk P, Kostulas V, et al. Multiple sclerosis and optic neuritis: CCR5 and CXCR3 expressing T cells are augmented in blood and cerebrospinal fluid. J Neurol. 2002;249(6):723–9.

49. Hanahan D, Weinberg R a. Hallmarks of cancer: The next generation. Cell. 2011;144(5):646–74.

50. Holm JS, Funt SA, Borch A, Munk KK, Bjerregaard AM, Reading JL, et al. Neoantigen-specific CD8 T cell responses in the peripheral blood following PD-L1 blockade might predict therapy outcome in metastatic urothelial carcinoma. Nat Commun. 2022;13(1).

51. Kristensen NP, Heeke C, Tvingsholm SA, Borch A, Draghi A, Crowther MD, et al. Neoantigen-reactive CD8+ T cells affect clinical outcome of adoptive cell therapy with tumor-infiltrating lymphocytes in melanoma. J Clin Invest. 2022;132(2).

52. Cloughesy TF, Mochizuki AY, Orpilla JR, Hugo W, Lee AH, Davidson TB, et al. Neoadjuvant anti-PD-1 immunotherapy promotes a survival benefit with intratumoral and systemic immune responses in recurrent glioblastoma. Nat Med. 2019;25(3).

53. Osa A, Uenami T, Koyama S, Fujimoto K, Okuzaki D, Takimoto T, et al. Clinical implications of monitoring nivolumab immunokinetics in non–small cell lung cancer patients. JCI Insight. 2018;3(19).

54. Duhen T, Duhen R, Montler R, Moses J, Moudgil T, De Miranda NF, et al. Co-expression of CD39 and CD103 identifies tumor-reactive CD8 T cells in human solid tumors. Nat Commun. 2018;9(1):1–13.

55. Simoni Y, Becht E, Fehlings M, Loh CY, Koo SL, Teng KWW, et al. Bystander CD8+ T cells are abundant and phenotypically distinct in human tumour infiltrates. Nature. 2018;557(7706).

56. Wolfl M, Kuball J, Ho WY, Nguyen H, Manley TJ, Bleakley M, et al. Activation-induced expression of CD137 permits detection, isolation, and expansion of the full repertoire of CD8+ T cells responding to antigen without requiring knowledge of epitope specificities. Blood. 2007;110(1):201–10.

57. Chow A, Uddin FZ, Liu M, Dobrin A, Nabet BY, Mangarin L, et al. The ectonucleotidase CD39 identifies tumor-reactive CD8+ T cells predictive of immune checkpoint blockade efficacy in human lung cancer. Immunity. 2023;56(1):93–106.

58. Kverneland AH, Chamberlain CA, Borch TH, Nielsen M, Mørk SK, Kjeldsen JW, et al. Adoptive cell therapy with tumor-infiltrating lymphocytes supported by checkpoint inhibition across multiple solid cancer types. J Immunother Cancer. 2021;9(10):3499.

59. Krishna S, Lowery FJ, Copeland AR, Bahadiroglu E, Mukherjee R, Jia L, et al. Stem-like CD8 T cells mediate response of adoptive cell immunotherapy against human cancer. Science (80-). 2020;370(6522):1328.

60. Kortekaas KE, Santegoets SJ, Sturm G, Ehsan I, van Egmond SL, Finotello F, et al. CD39 identifies the CD4+ tumor-specific T-cell population in human cancer. Cancer Immunol Res. 2020;8(10):1311–21.

61. Voskoboinik I, Smyth MJ, Trapani JA. Perforin-mediated target-cell death and immune homeostasis. Vol. 6, Nature Reviews Immunology. 2006.

62. Zheng C, Zheng L, Yoo JK, Guo H, Zhang Y, Guo X, et al. Landscape of Infiltrating T Cells in Liver Cancer Revealed by Single-Cell Sequencing. Cell. 2017;169(7).

63. Kim KH, Kim HK, Kim HD, Kim CG, Lee H, Han JW, et al. PD-1 blockade-unresponsive human tumor-infiltrating CD8+ T cells are marked by loss of CD28 expression and rescued by IL-15. Cell Mol Immunol. 2021;18(2).

64. Kamphorst AO, Wieland A, Nasti T, Yang S, Zhang R, Barber DL, et al. Rescue of exhausted CD8 T cells by PD-1 targeted therapies is CD28-dependent. Science (80-). 2017;355(6332):1423.

65. Hui E, Cheung J, Zhu J, Su X, Taylor MJ, Wallweber HA, et al. T cell costimulatory receptor CD28 is a primary target for PD-1-mediated inhibition. Science (80-). 2017;355(6332):1428–33.

66. Woroniecka K, Chongsathidkiet P, Rhodin K, Kemeny H, Dechant C, Harrison Farber S, et al. T-cell exhaustion signatures vary with tumor type and are severe in glioblastoma. Clin Cancer Res. 2018;24(17).

67. Davidson TB, Lee A, Hsu M, Sedighim S, Orpilla J, Treger J, et al. Expression of PD-1 by T cells in malignant glioma patients reflects exhaustion and activation. Clin Cancer Res. 2019;25(6).

68. Jenkins RW, Barbie DA, Flaherty KT. Mechanisms of resistance to immune checkpoint inhibitors. Br J Cancer. 2018;118(1).

69. Hung AL, Maxwell R, Theodros D, Belcaid Z, Mathios D, Luksik AS, et al. TIGIT and PD-1 dual checkpoint blockade enhances antitumor immunity and survival in GBM. Oncoimmunology. 2018;7(8).

70. Raphael I, Kumar R, McCarl LH, Shoger K, Wang L, Sandlesh P, et al. TIGIT and PD-1 Immune Checkpoint Pathways Are Associated With Patient Outcome and Anti-Tumor Immunity in Glioblastoma. Front Immunol. 2021;12.

71. Cendrowski J, Mamińska A, Miaczynska M. Endocytic regulation of cytokine receptor signaling. Cytokine Growth Factor Rev. 2016;32:63–73.

72. Saad E Ben, Oroya A, Rudd CE. Abstract 6528: Anti-PD-1 induces the endocytosis of the co-receptor from the surface of T-cells: Nivolumab is more effective than Pembrolizumab. Cancer Res. 2020;80(16_Supplement).

73. Lee AH, Sun L, Mochizuki AY, Reynoso JG, Orpilla J, Chow F, et al. Neoadjuvant PD-1 blockade induces T cell and cDC1 activation but fails to overcome the immunosuppressive tumor associated macrophages in recurrent glioblastoma. Nat Commun. 2021;12(1).

74. De Groot J, Penas-Prado M, Alfaro-Munoz K, Hunter K, Pei BL, O'Brien B, et al. Window-of-opportunity clinical trial of pembrolizumab in patients with recurrent glioblastoma reveals predominance of immune-suppressive macrophages. Neuro Oncol. 2020;22(4).

75. Lu Y, Ng AHC, Chow FE, Everson RG, Helmink BA, Tetzlaff MT, et al. Resolution of tissue signatures of therapy response in patients with recurrent GBM treated with neoadjuvant anti-PD1. Nat Commun. 2021;12(1).

76. Donia M, Hansen M, Sendrup SL, Iversen TZ, Ellebæk E, Andersen MH, et al. Methods to improve adoptive T-cell therapy for melanoma: IFN-γ enhances anticancer responses of cell products for infusion. J Invest Dermatol. 2013;133(2).

77. Dhatchinamoorthy K, Colbert JD, Rock KL. Cancer Immune Evasion Through Loss of MHC Class I Antigen Presentation. Front Immunol. 2021;12.

78. Lee MY, Jeon JW, Sievers C, Allen CT. Antigen processing and presentation in cancer immunotherapy. J Immunother cancer. 2020;8(2).

79. Scheer M, Leisz S, Sorge E, Storozhuk O, Prell J, Ho I, et al. Neurofibromatosis type 1 gene alterations define specific features of a subset of glioblastomas. Int J Mol Sci. 2022;23(1).

80. Lobbous M, Bernstock JD, Coffee E, Friedman GK, Metrock LK, Chagoya G, et al. An update on neurofibromatosis type 1-associated gliomas. Cancers (Basel). 2020;12(1).

81. Zhang J, Caruso FP, Sa JK, Justesen S, Nam DH, Sims P, et al. The combination of neoantigen quality and T lymphocyte infiltrates identifies glioblastomas with the longest survival. Commun Biol. 2019;2(1).

82. Hilf N, Kuttruff-Coqui S, Frenzel K, Bukur V, Stevanović S, Gouttefangeas C, et al. Actively personalized vaccination trial for newly diagnosed glioblastoma. Nature. 2019;565(7738).

83. Keskin DB, Anandappa AJ, Sun J, Tirosh I, Mathewson ND, Li S, et al. Neoantigen vaccine generates intratumoral T cell responses in phase Ib glioblastoma trial. Nature. 2019;565(7738).

84. Leko V, Cafri G, Yossef R, Paria B, Hill V, Gurusamy D, et al. Identification of neoantigen-reactive T lymphocytes in the peripheral blood of a patient with glioblastoma. J Immunother Cancer. 2021;9(7).

Figure Legends

Figure 1 Clinical setup and survival. a) Timeline showing administration of treatment with Nivolumab (nivo) and Bevacizumab (beva), including timepoints of sampling blood and tumor. Treated patients (blue) included a surgical group and non-surgical group, and all patients received Nivolumab and Bevacizumab every two weeks. Patients in the surgical group also received Nivolumab seven days prior surgery. Control patients (purple) with recurrent glioblastoma undergoing neurosurgical resection were additionally included. These patients did not receive Nivolumab before resection. Additionally, blood samples were collected from treated patients at Day 0 as baseline (BL), after 8 weeks (WK 8) and 16 weeks (WK 16). An additional blood sample was collected from patients in surgical group 3 weeks (WK 3) after Nivolumab administration (2 weeks after surgery). **b-e)** Overall survival by Kaplan-Meier curves comparing patients in our CA209-9UP clinical trial (N=40, black line) with a historical patient group (N=156, grey line) from our one-site database, who were treated with bevacizumab and irinotecan from 2006-2014, but not Nivolumab. All patients were subdivided into **b-c)** a surgical group and **d-e)** a non-surgical group. Comparison between the historical patient group and the patient in trial was done **b&d)** without using propensity scores and **c&e)** weighted using propensity scores based on age, gender, corticosteroid use, multifocal disease, MGMT status and extent of resection.

Figure 2 Intratumoral detection of Nivolumab and tissue resident T cells. a) shows an illustrative explanation of PD1 and Nivolumab antibody (Ab)-detection; Nivolumab bound to PD1 was detected with a fluorochrome-conjugated anti-IgG4 Ab (red) binding to the Fc region of Nivolumab (black Ab), while free PD1 molecules were detected with fluorochrome-labelled anti-PD1 Ab (yellow) by flow cytometry. **b)** Explanation of dot plots showing Nivolumab binding and saturation (left), representative flow cytometry dot plots of unrested and rested tumor digest stained with anti-PD1 and anti-IgG4, showing a complete Nivolumab saturation of intratumoral T-cells in unrested tumor digest from Nivolumab-treated (NIVO) patient, which is partly lost after resting. Intratumoral T-cells from control (CTRL) patients do not bind anti-IgG4 (right). **c)** Frequency of CD8+ T-cells stained with anti-IgG4 (Nivolumab bound) and anti-PD1 (free PD1 molecules) in unrested (light grey) and rested (dark grey) tumor digest (NIVO N = 6, CTRL N = 4). **d)** Frequency of CD8+ and CD4+ T cells co-expressing the markers of tissue residency, CD69 and CD103, in Tumor digest from NIVO patients (light blue) and CTRL patients (purple) (left) (CD8 NIVO N = 14, CD8 CTRL N = 10 , CD4 NIVO N = 15 , CD4 CTRL N = 10). Representative plot of intratumoral CD8+ T-cells expressing CD69 and CD103 (right). **e)** Frequency of CD8+ and CD4+ T-cells binding Nivolumab (anti-IgG4) that are tissue-resident T cells (CD8 NIVO N = 12, CD8 CTRL N = 10, CD4 NIVO N = 14 , CD4 CTRL N = 10). **f)** Representative plots from NIVO and CTRL patients showing tissue resident CD8+ T-cells from rested tumor digest binding anti-PD1 and anti-IgG4. For bar plots indicated the mean and error bars shows SD. Means were compared between NIVO and CTRL using unpaired t-test. * = $p<0.05$, ** = $p<0.01$, *** = $p<0.001$, **** = $p<0.0001$.

Figure 3 CNS-homing, activation and proliferation in tumor tissue and blood. a-j) The frequency of intratumoral T cells expressing different markers for migration, activation and proliferation was detected by flow cytrometry to compare the distribution of these within the GBM tumor of Nivolumab treated patients and control patients. **a)** Firstly, the frequency of CD4 and CD8 T cells within the intratumoral T cell population (CD8 NIVO N = 20, CD8 CTRL N = 10, CD4 NIVO N = 20, CD4 CTRL N = 10). **b)** Frequency of CD8+ and CD4+ T-cells co-expressing the chemokine receptors, CD183 (CXCR3) and CD195 (CCR5) in tumor tissue of Nivolumab-treated (NIVO) and control (CTRL) patients, for indication of

CNS homing (CD8 NIVO N = 12, CD8 CTRL N = 10 , CD4 NIVO N = 14 , CD4 CTRL N = 10). **c-d)** The frequency of CD4+ and CD8+ T-cells high positive for CD183 (CD8 NIVO N = 15, CD8 CTRL N = 10 , CD4 NIVO N = 15 , CD4 CTRL N = 10) and CD195 (CD8 NIVO N = 12, CD8 CTRL N = 10 , CD4 NIVO N = 14 , CD4 CTRL N = 10), respectively, detected to compare the expression level of the chemokine receptors on intratumoral T cells in NIVO and control patients. **e)** Representative flow cytometry plot of Ab staining of tumor digest from NIVO and CTRL patients. Gating for T cells expressing high levels of chemokine receptors (CD183 and CD195) is marked with red. **f)** Frequency of CD8+ T-cells co-expressing CD183 and CD195 in blood samples from Baseline (BL) (Surgical N = 11, Non-surgical N = 14), week (WK) 8 (Surgical N = 9, Non-surgical N = 11) and WK16 (Surgical N = 5, Non-surgical N = 3). Frequencies are compared between the surgical group and the tumor-bearing group (non-surgical group). **g)** Frequency of T cells expressing Ki67 among intratumoral CD8+ and CD4+ T-cells (CD8 NIVO N = 13, CD8 CTRL N = 10, CD4 NIVO N = 14 , CD4 CTRL N = 10). **h)** Frequency of T-cells expressing CD28 among intratumoral CD8+ and CD4+ T-cells (CD8 NIVO N = 14, CD8 CTRL N = 10, CD4 NIVO N = 15, CD4 CTRL N = 10). **i)** Frequency of tissue resident T-cells expressing CD39 among intratumoral CD8+ and CD4+ T-cells (CD8 NIVO N = 14, CD8 CTRL N = 10, CD4 NIVO N = 15, CD4 CTRL N = 10). **j)** Frequency of tissue resident T-cells expressing CD137 among intratumoral CD8+ and CD4+ T-cells (CD8 NIVO N = 14, CD8 CTRL N = 10, CD4 NIVO N = 15, CD4 CTRL N = 10). For bar plots indicated the mean and error bars shows SD. Means were compared between NIVO and CTRL (Tumor), and between the surgical group and the tumor-bearing group (non-surgical group), and the four time points (blood) using unpaired t-test. * = $p<0.05$, ** = $p<0.01$, *** = $p<0.001$, **** = $p<0.0001$. **k)** Volcano plot showing 1,716 differential overexpressed genes and 260 under-expressed genes in NIVO patients (N = 20) compared to control patients (N = 10) based on bulk transcriptomic data. Overexpressed genes in NIVO are shown in red with an adjusted p-value < 0.05 and log2 fold change > 2, underexpressed genes in NIVO patients are shown blue with adjusted p-value < 0.05 and log2 fold change < -2. The highlighted genes cover the most up- and down regulated genes and few immune-related genes of interest. Genes assed by flow cytometry are additionally marked.

Figure 4 Nivolumab induce late differentiation of T-cells and an anti-inflammatory TME. a-d) Frequency of intratumoral CD8+ T-cells from NIVO and CTRL patients expressing inhibitory markers detected by flow cytometry; TIGIT (CD8 NIVO N = 12, CD8 CTRL N = 10 , CD4 NIVO N = 12, CD4 CTRL N = 10) (a), LAG-3 (b), TIM-3 (c), CTLA-4 (d) (CD8 NIVO N = 13, CD8 CTRL N = 10 , CD4 NIVO N = 14, CD4 CTRL N = 10). **e)** Pie chart showing the proportion of intratumoral T cells expressing one or more of the studied inhibitory molecules (TIGIT, LAG-3, CTLA-4, TIM-3) within the Nivolumab treated patients (NIVO) (N = 12) and the control patients (CTRL) (N = 10), respectively. The pie charts are divided in negative cells (grey), single positive (green), double positive (purple), triple positive (blue) and quadruple positive cells (yellow). **f)** Frequency of Treg cells among intratumoral CD4+ T-cells from NIVO and CTRL patients (CD8 NIVO N = 13, CD8 CTRL N = 10, CD4 NIVO N = 14, CD4 CTRL N = 10). **g)** Frequency of CD8+ T-cells expressing TIGIT from blood samples at baseline (BL) (Surgical N = 11, Non-surgical N = 14), week (WK) 8 (Surgical N = 9, Non-surgical N = 11) and WK16 (Surgical N = 5, Non-surgical N = 3). Comparing the surgical group to the tumor bearing group (non-surgical) group. **h)** Frequency of the collected PD1+ population (based on anti-PD1 and anti-IgG4 staining) within intratumoral T-cells from Nivolumab-treated (NIVO) and control (CTRL) patients (CD8 NIVO N = 12, CD8 CTRL N = 10, CD4 NIVO N = 14, CD4 CTRL N = 10). **i)** Frequency of a collected PD1+ population within PBMC derived T-cells collected at different time points of the treatment, before (BL) (N = 24) and after (WK3 N = 8, WK8 N = 20, WK16 N = 8) Nivolumab administration. **j)** The kinetics of Nivolumab binding. CD8+ T-cells derived from blood collected before (BL) (IgG4 N = 23, PD1 N = 39) and after (WK3 IgG4 N = 8, PD1 N = 16; WK8 IgG4 N = 19,

PD1 N = 30; WK16 IgG4 N = 8, PD1 N = 13) Nivolumab administration stained with anti-PD1 (yellow) and anti-IgG4 (red), points represents mean and error bars shows SD. For bar plots indicated the mean and error bars shows SD. Means were compared between NIVO and CTRL (Tumor), the surgical group and the tumor-bearing group (non-surgical group), and the four time points (blood) using unpaired t-test. * = p<0.05, ** = p<0.01, *** = p<0.001, **** = p<0.0001.

Figure 5 Comparison of patients with reactive T-cells versus non-reactive T-cells. a) Reactivity towards autologous tumor digest detected in CD8 (N = 14) and CD4 (N = 15) REP TILs. TILs were co-cultured with autologous tumor digest for 8 hours and hereafter intracellularly stained for TFN-α, IFN-γ, CD137 and surface stained for CD107a. TILs expressing at least two of the markers, where defined as reactive. Background reactivity (TILs alone) is subtracted and hereafter patients with more than 1% reactive TILs are defined as reactive. Patients with tumor reactive TILs are highlighted in red. Patients without tumor reactive TILs are marked in grey. **b)** 372 differential over-expressed and 1,150 differential under-expressed genes were found in patients with reactive T-cells by differential expression analysis with adjusted p-value < 0.05. These differentially expressed genes are illustrated by a heatmap showing that patients with reactive (N = 4) and non-reactive (N = 16) T-cells were defining the two first unsupervised clusters. The highlighted genes consist of the most up- and down regulated genes and include some immune-related genes of interest. **c)** A gene set enrichment analysis was made from the DEA and "antigen presentation on MHC-I" was found as an enriched pathway for patients with reactive T-cells.

Figure 6 Detection of neo-antigen reactive CD8+ T-cells (NARTs). a) Illustrative explanation of NART detection**.** Neoantigens were predicted based on whole exome sequencing (WES) and RNA sequencing of tumor and WES of healthy tissue (blood). A patient specific panel of DNA-barcoded pMHC multimers, was assembled with the predicted neopeptides and virus peptides. Patient material (TILs and PBMCs) was stained with a pool of the multimer panel, and multimer+ CD8+ T-cells were sorted based on their fluorochrome label; PE (blue) for neopeptides and APC (red) for virus peptides. The DNA-barcodes bound to the sorted T-cells were hereafter amplified by PCR and sequenced. Enriched and hereby immunogenic neopeptide- and virus peptide-MHC complexes were identified based on the corresponding DNA-barcode. **b)** Screening output for patient NVB02 and NVB05. Significantly enriched (p < 0.001, Log2 fold change > 2) barcoded pMHC multimers are colored and labelled with the immunogenic peptide sequence. Virus antigens are marked in red and neoantigens are marked in blue. The dot size represents an estimated frequency of CD8+ T-cells for each neoantigen reactive CD8+ T cell (NART). Grey dots are all pMHC multimers that where not significantly enriched after sample staining. Specificities are shown for each blood sample timepoint; Baseline (BL), week (WK) 3, WK8, WK16, and for both young TILs (YTIL) and rapidly expanded (REP) TILs. The screened pMHC are additionally divided based on HLA type. **c)** Number of responses towards different neoantigens (blue) and virus antigens (red). Individual patients are marked in different shades of the respective color. The plot is further divided in PBMC and TILs. There was no significant difference between blood-sample time points or between YTILs and REP TILs **d)** Sum of estimated frequency of NARTs shown in percentage out of all CD8+ T-cells recognizing different neoantigens (blue) and virus antigens (red). There was also no significant difference between blood sample time points or between YTILs and REP TILs.

Figure 1

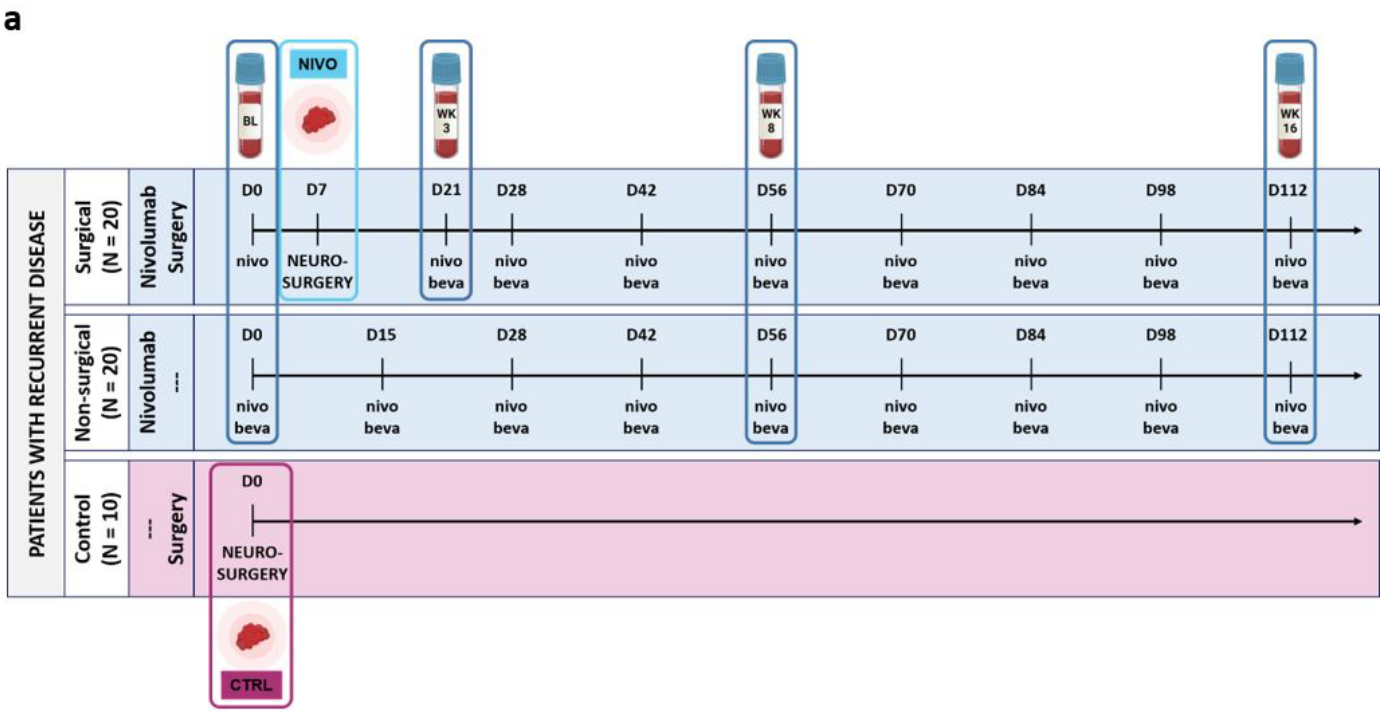

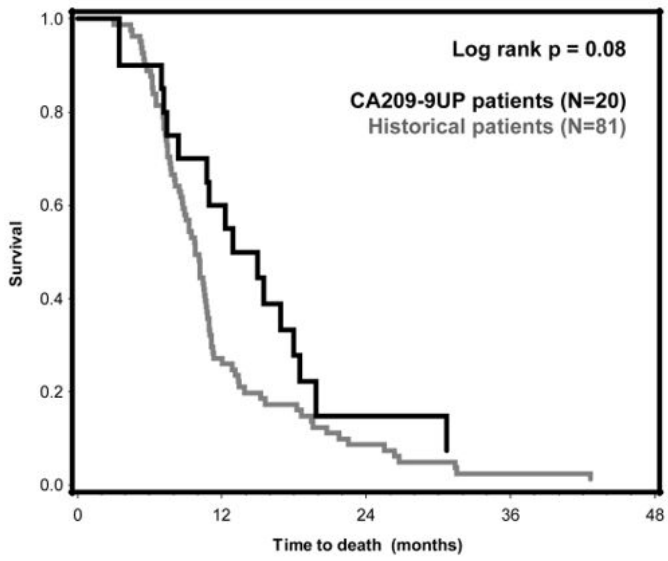

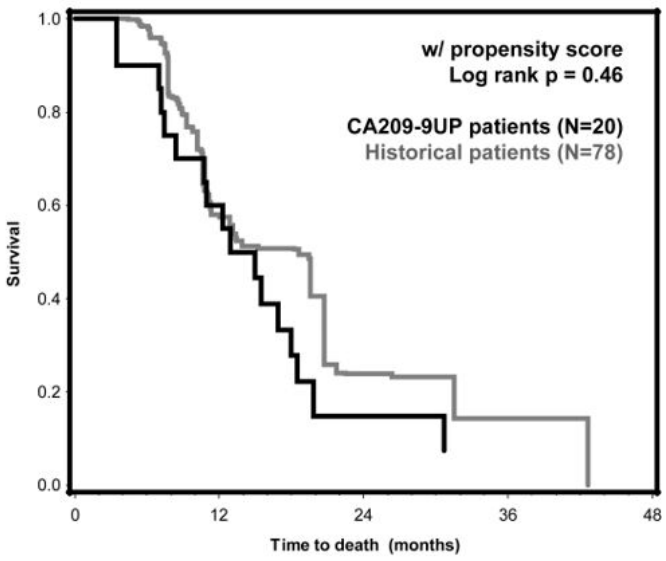

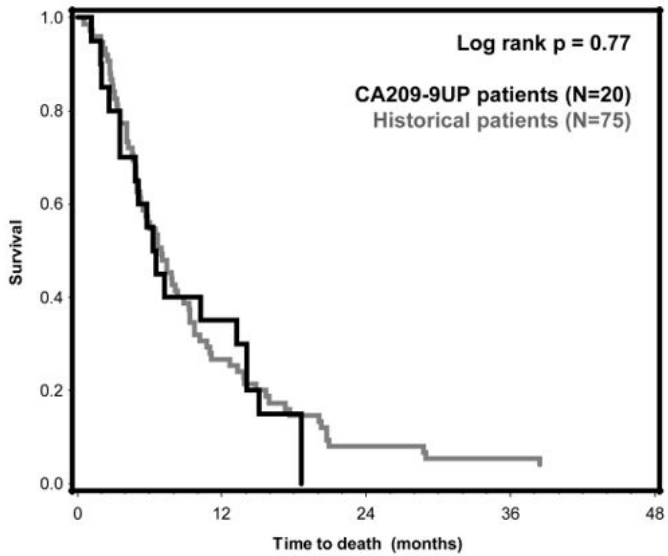

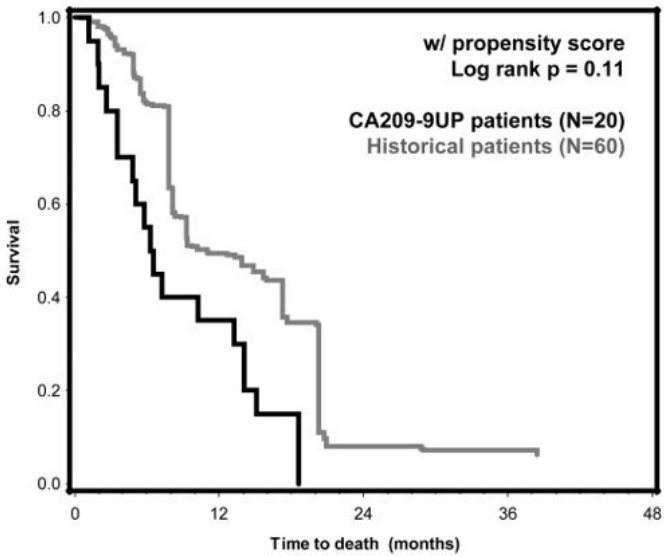

Figure 2

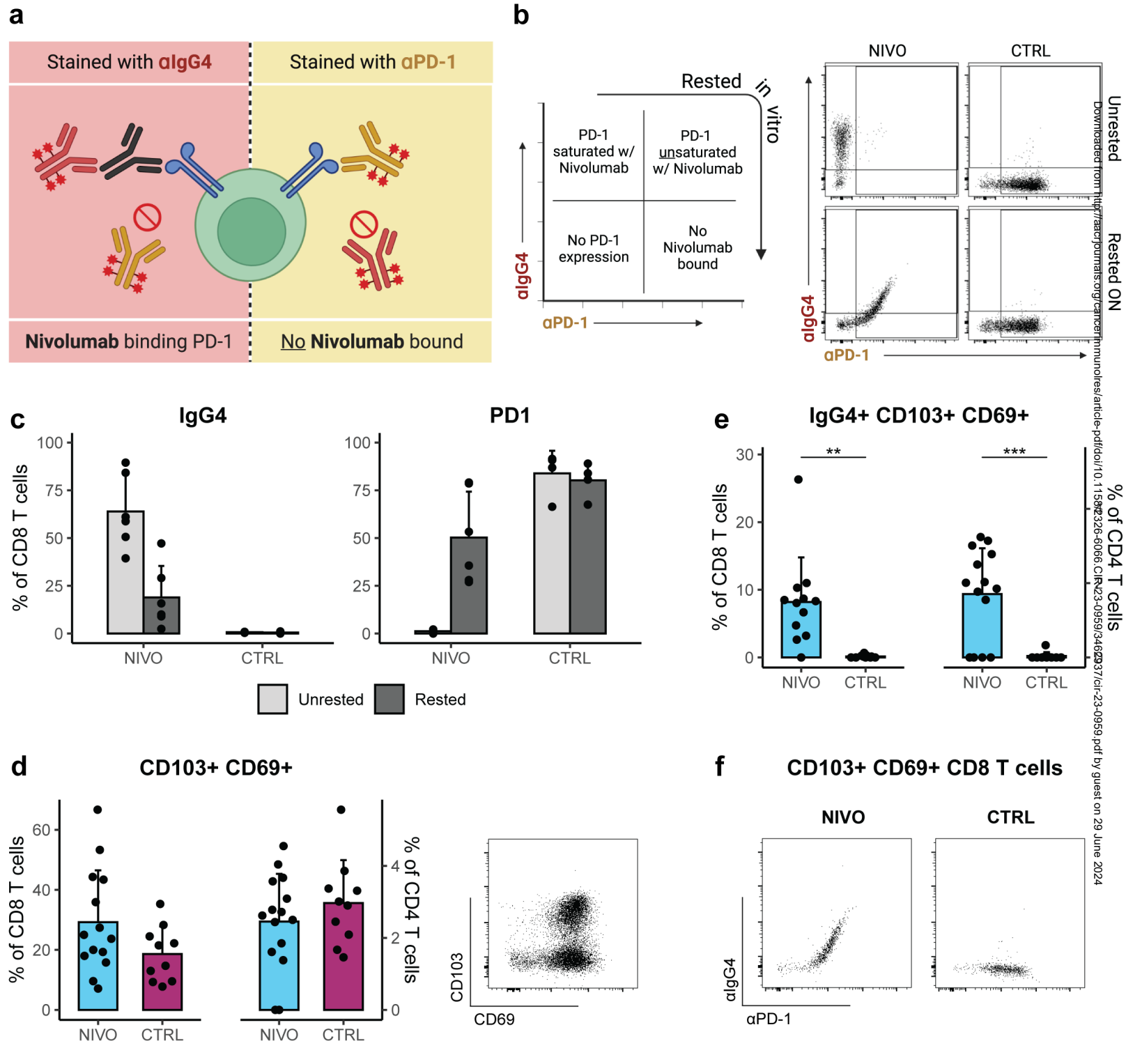

Figure 3

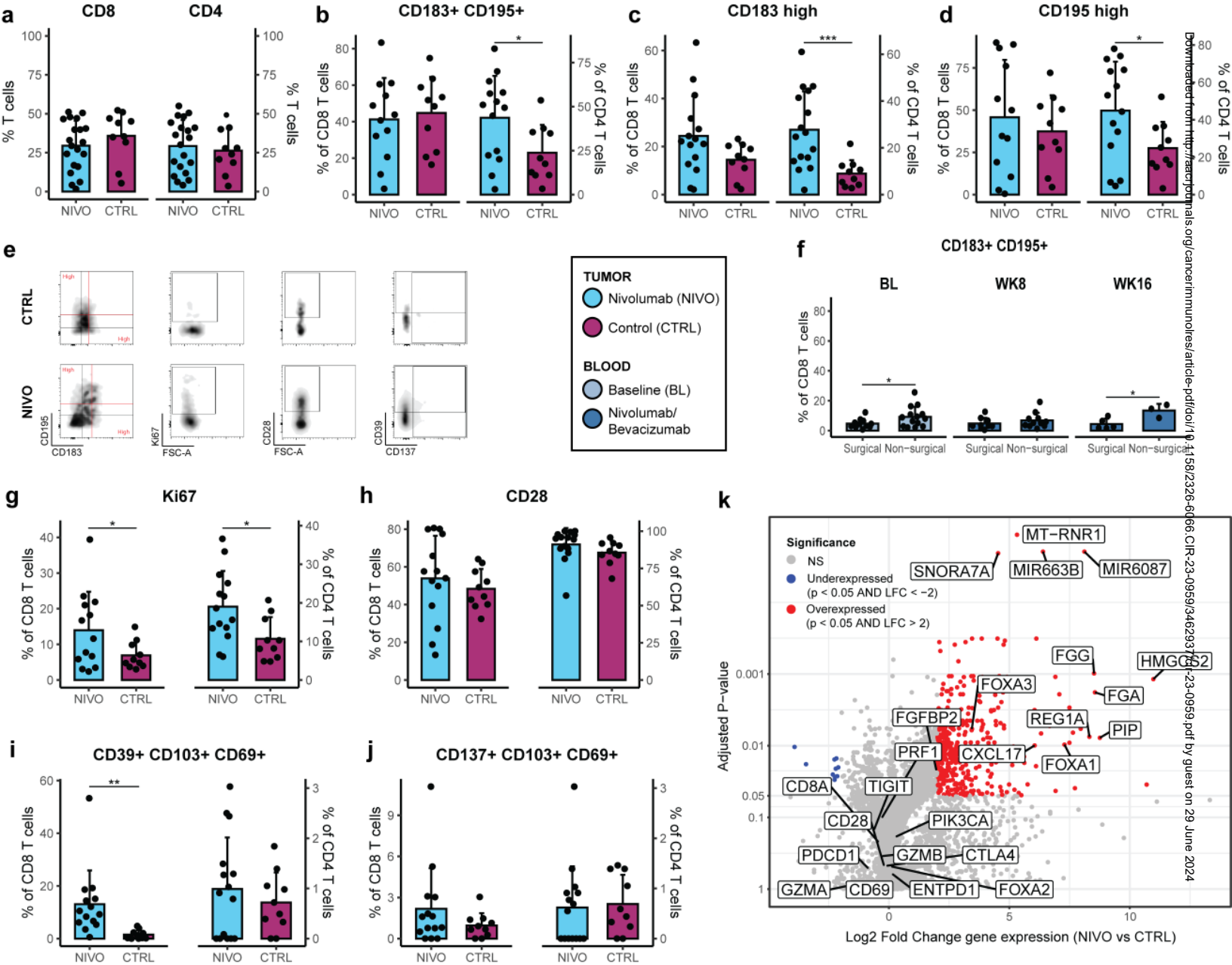

Figure 4

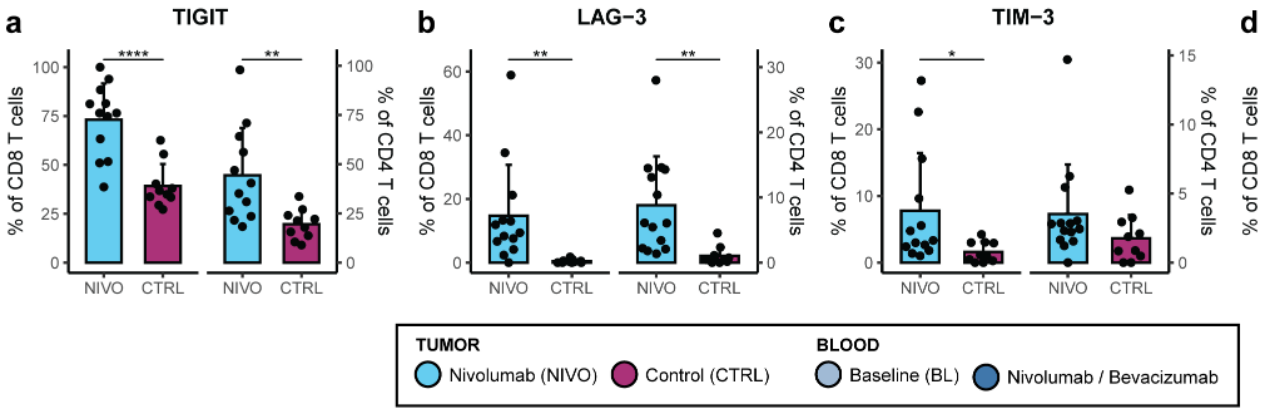

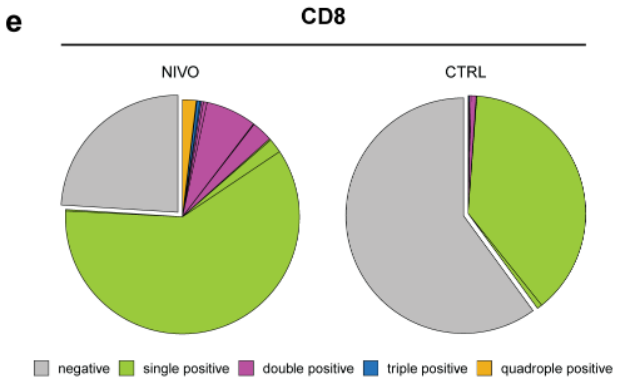

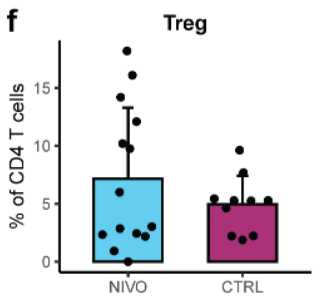

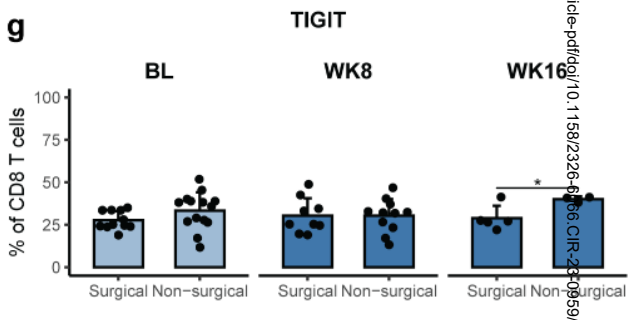

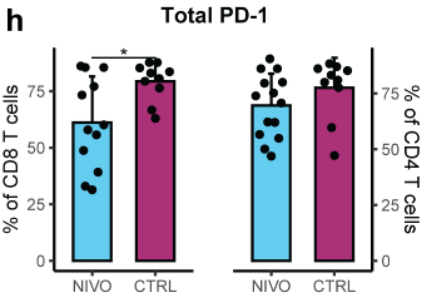

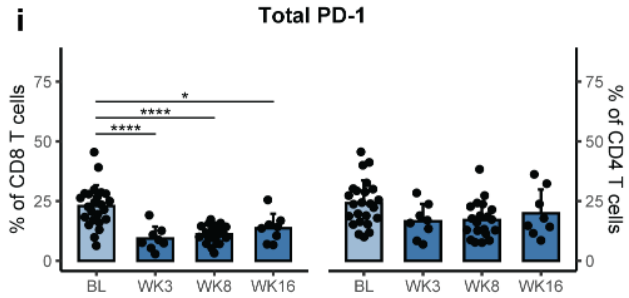

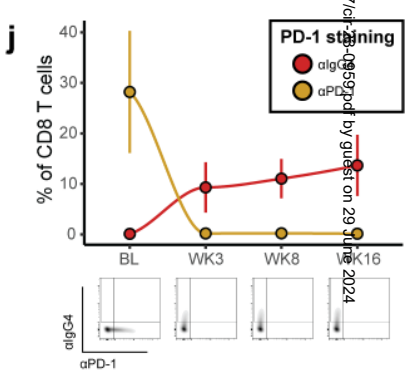

Figure 5

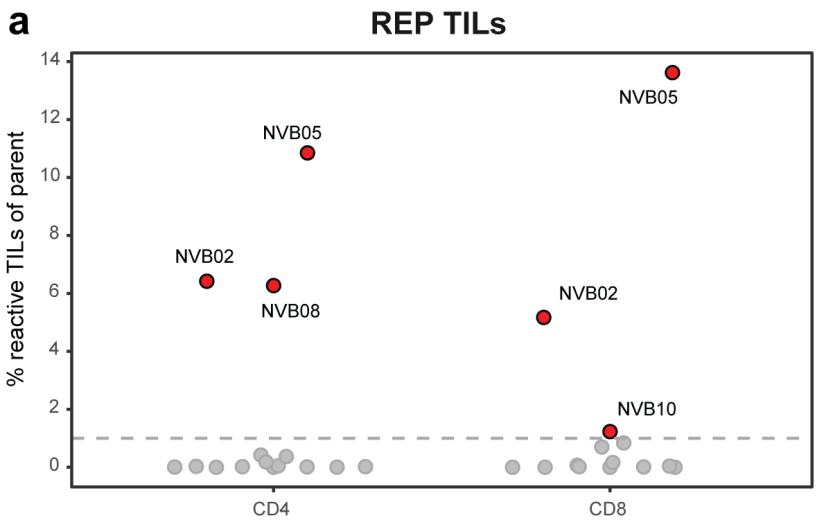

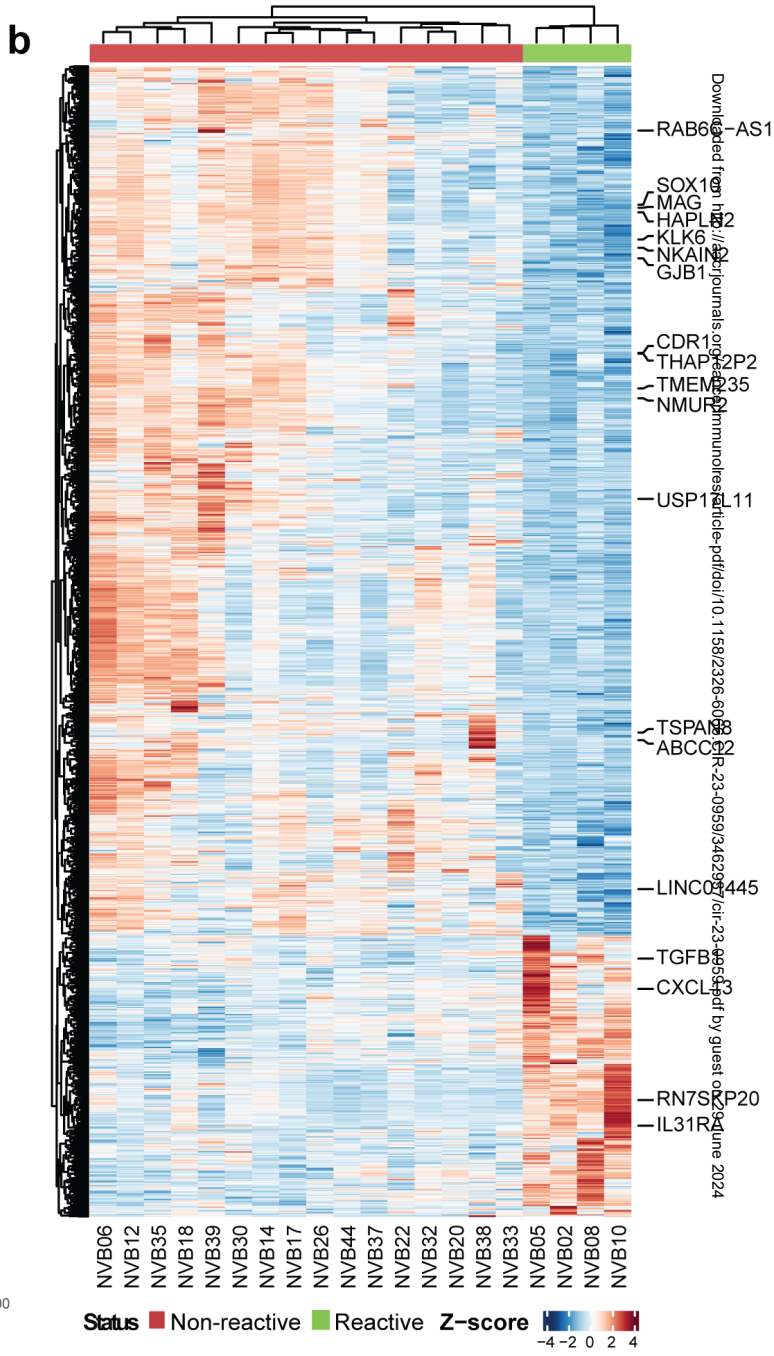

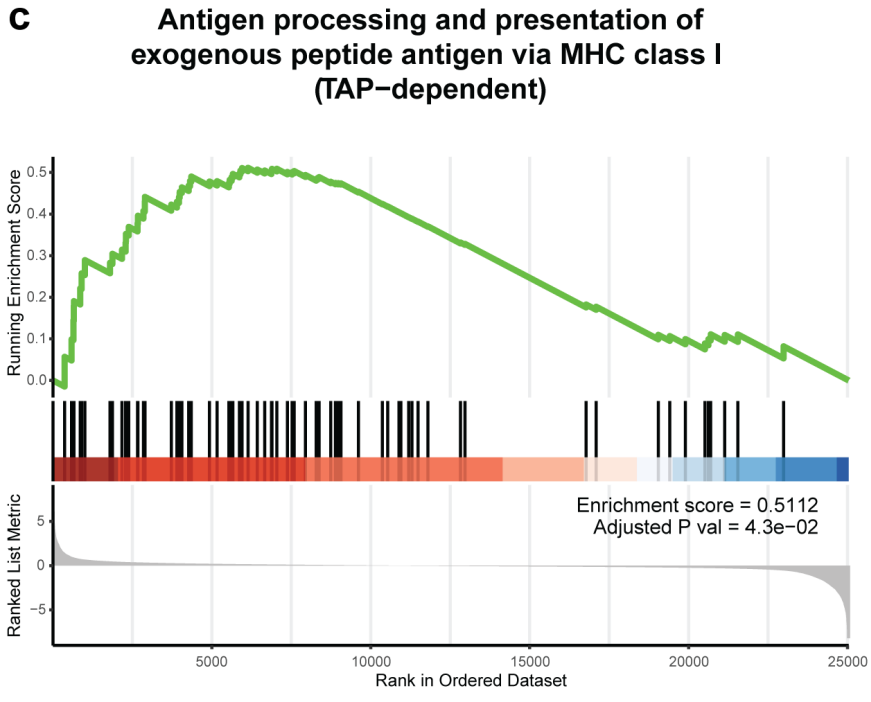

Figure 6